A Comparison Between XFEM and SPH in Solving Two-dimensional Fracture Mechanics Problems, with Applications in Food Breakdown Modeling

by

Baharan Pourahmadi-Meibodi

B.Sc., University of Tehran, 2016

A THESIS SUBMITTED IN PARTIAL FULFILLMENT OF

THE REQUIREMENTS FOR THE DEGREE OF

MASTER OF APPLIED SCIENCE

in

THE FACULTY OF GRADUATE AND POSTDOCTORAL STUDIES

(Biomedical Engineering)

THE UNIVERSITY OF BRITISH COLUMBIA

(Vancouver)

February 2020

The following individuals certify that they have read, and recommend to the Faculty of Graduate and Postdoctoral Studies for acceptance, a thesis/dissertation entitled:

A Comparison Between XFEM and SPH in Solving Two-dimensional Fracture Mechanics Problems, with Applications in Food Breakdown Modeling

submitted by Baharan Pourahmadi-Meibodi in partial fulfillment of the requirements for

the degree of Master of Applied Science

In Biomedical Engineering

Examining Committee:

Dr. Sidney Fels
Supervisor

Dr. Dana Grecov
Supervisory Committee Member

Dr. Robert Rohling
Supervisory Committee Member

Abstract

Masticatory performance and the occlusal force are two of the main clinical metrics that are used to evaluate the masticatory function objectively. A comprehensive evaluation of masticatory function requires a correlative inspection of these two metrics. The complex multi-variant nature of the human mastication and the limitations of visualization and clinical measurement techniques, complicates the clinical investigation of masticatory function. A biomechanical model of oral food breakdown has the ability to bypass these difficulties. The currently available food breakdown models are either highly dependent on experimental data or are focused on food engineering applications. In this thesis, we attempted to solve these issues by building a two-dimensional fracture mechanics model to simulate the oral food breakdown. The different computational methods available to solve fracture mechanics problems have limits and strengths, which affects the accuracy of their solution. Extended Finite Element Method (XFEM) and Smoothed Particle Hydrodynamics (SPH) method use two very distinct approaches to solve fracture mechanics problems; comparing the effectiveness of these two methods can provide valuable insights into the computational possibilities. As the classical SPH formulation for solid mechanics suffers from numerical deficiencies, we first performed a set of modifications to build a corrected SPH model for solid and fracture mechanics. We solved fracture mechanics benchmark tests using XFEM and the modified version of SPH and investigated their strengths and weaknesses thoroughly. The SPH method eventually was selected to model the food breakdown procedure. We simulated the food breakdown following one chewing stroke using our two-dimensional SPH fracture model and measured the corresponding occlusal force and masticatory performance for a range of different food properties. The food breakdown model was able to simulate the experimental correlation

between masticatory performance and the food properties. Although the simulated measurements for occlusal force were in accordance with the previous experimental studies, further detailed clinical investigation is required to validate the force pattern during chewing. The simplified biomechanical model of oral food comminution described in this work can be regarded as the first step toward building a patient-specific model to pre-assess the patient's masticatory function following a maxillofacial reconstructive surgical plan.

Lay Summary

The complexity of the human chewing system and the deficiency of the available clinical measurement techniques in addressing this complexity, hinder the evaluation procedure of the chewing function.

In this work, we used the principles of fracture mechanics to build a simplified food breakdown model that is able to evaluate the masticatory function by measuring the relevant clinical metrics. To build this model, the available computational methods that are used to solve such fracture mechanics problems were modified and compared against each other to guarantee the accuracy of the solution.

The simulated results from our food breakdown model are in accordance with the clinical measurements of masticatory function.

Preface

The contributions and results from Chapter 3 have been partly presented at CMBBE 2018 [P1]. The numerical modifications and the numerical studies presented in Chapter 3 were designed and performed by myself, under the supervision of Prof. Sidney Fels.

The contributions and results from Chapter 4 have been partly presented at ISB 2019 [P2]. The food breakdown model, the method to measure the masticatory performance and the occlusal force, and the relevant validation studies were designed and performed by myself, under the supervision of Prof. Sidney Fels.

Conference presentations:

[P1]: B.Pourahmadi et al., Investigation of efficient computational techniques for food breakdown modeling. *Presented at CMBBE 2018, Lisbon.*

[P2]: B.Pourahmadi et al., Assessing the masticatory function using a food breakdown model. *Presented at ISB 2019, Calgary.*

Table of Contents

List of Tables

List of Figures

List of Symbols

σ: Stress

ϵ: Strain

ν: Poisson's ratio

E: Modulus of elasticity

K: Stress intensity factor (SIF)

G: Griffith crack growth energy

Π: Potential energy

m: Mass

ρ: Density

W: Smoothing function

h: Smoothing length

c: Speed of sound

$\widetilde{U}$: Potential energy per thickness

ψ: Discontinuous enrichment function

γ_s: Surface energy

R: Artificial stress tensor

ϕ: Contact potential

D: Damage parameter

C_g: Crack growth speed

List of Abbreviations

ATM: Anterior Tongue Movement

CFL: Courant-Friedrichs-Lewy

DEM: Discrete Element Method

EMG: Electromyography

FEM: Finite Element Method

LEFM: Linear Elastic Fracture Mechanics

NSPH: Normalized Smoothed Particle Hydrodynamics

ODE: Ordinary Differential Equation

PDE: Partial Differential Equation

SIF: Stress Intensity Factor

SPH: Smoothed Particles Hydrodynamics

XFEM: Extended Finite Element Method

2D: Two-dimensional

3D: Three-dimensional

Acknowledgements

During the past few years, I had the opportunity to work with an amazing group at the HCT lab. It was an honor, and more importantly, a great pleasure to be part of this team. In particular, I want to express my gratitude to my supervisor, Dr. Sidney Fels: I learnt a lot from you, thank you.

I also want to say a thank you to all my friends: “*The world is a small place, I wish it was smaller*.”

Lastly, a big thank you to my parents for their never-ending and unconditional love and support.

MENA,

This is for you,

and your restless soul.

Chapter 1: Introduction

Chewing, or *mastication*, is one of the most important functions of the oral system. Numerous types of oral cavity and maxillofacial disorders can affect the efficiency of the masticatory function in patients. The masticatory ability of the healthy subjects has been widely studied in order to provide a standard for clinicians to investigate the clinical outcomes from different patient groups and to plan the treatment properly.

Masticatory function can be investigated objectively by measuring the ability of the chewing system in comminuting the food morsels into smaller fragments, and subjectively based on patients' satisfaction.

Self-assessed masticatory function is determined using questionnaires and interviewing the patients [1]. Although the self-assessment methods are required to represent the patients' *perception*, previous clinical studies have indicated that these methods are not able to explain the mechanisms of chewing process and that the objective methods are required to properly plan the treatment [2].

1.1 Objective methods for assessment of masticatory function: what are we looking for?

There are multiple methodologies available to measure the different aspects of chewing ability objectively. *Masticatory performance*, one of the most common clinical measures, aims to evaluate the ability of the masticatory system to comminute food particles [3]. The exact definition of masticatory performance varies among different research works. In this work, 4-4 represents the definition of the masticatory performance. More details on the suitability of this particular definition is provided in 4.2.2.

Occlusal force, defined as the force exerted on the opposing teeth when the jaws are closed or tightened, is another major indicator of chewing function and a biomechanical input to the maxillofacial system. Occlusal force pattern on mandible is closely linked to the patients' chewing experience; altering the natural force pattern can lower the satisfaction with mastication [4]. Although a variety of methods and devices has been invented to measure the maximum voluntary bite force, assessing the actual occlusal force distribution on mandible during chewing remains a big challenge.

Masticatory performance together with the occlusal force pattern on the mandible can provide some essential understanding of the chewing functionality. However, the difficulty associated with the clinical measurement procedure due to the complexity of masticatory process, complicates the evaluation of the masticatory ability. Biomechanical modeling, a powerful computational tool, has the potential to facilitate this investigation.

1.2 Food breakdown modeling: how are we going to solve the problem?

Biomechanical modeling of the masticatory system has the ability to provide detailed information that is difficult to obtain experimentally. Although food and oral cavity interactions have a major influence on the mastication, most of the previous biomechanical modeling studies have neglected the food breakdown component and have simplified its effects to a single force vector acting on the dentition or considered food as an elastic material [5]. Computational modeling of oral food breakage is an important component missing in the previous studies. An accurate numerical representation of food breakdown can facilitate the assessment of the patients' chewing function. Previous works on food breakdown modeling (2.5) were focused on food engineering applications such as taste and aroma releasing process and the perception of food texture [6]. Although they provide a valuable understanding of the subject, a different modeling approach, particularly targeting the masticatory function, has to be implemented. Specifically speaking, the desired computational food breakdown model should be capable of assessing the masticatory performance and the occlusal force pattern. This requires a detailed review of the breakage mechanism and physics as well as the available computational methods to represent it.

1.3 Fracture mechanics

Fracture mechanics is the field that studies the manner in which materials break down under excessive loading and how cracks propagate through a solid body. A fracture mechanics model can be used to study the damage process of the food particles. Specifically speaking, a fracture mechanics model is capable of measuring the masticatory performance (by measuring the food fragment size following a chewing stroke) and the occlusal force (by measuring the stress distribution). More details on how to measure the masticatory performance and the occlusal force will be presented in 4.2.

In this work, a simplified fracture mechanics model is proposed to simulate the food breakdown. The assumptions and the simplifications that are made in this modeling work are presented in 1.3.1. Figure 1-1 schematically represents our simplified food breakdown model.

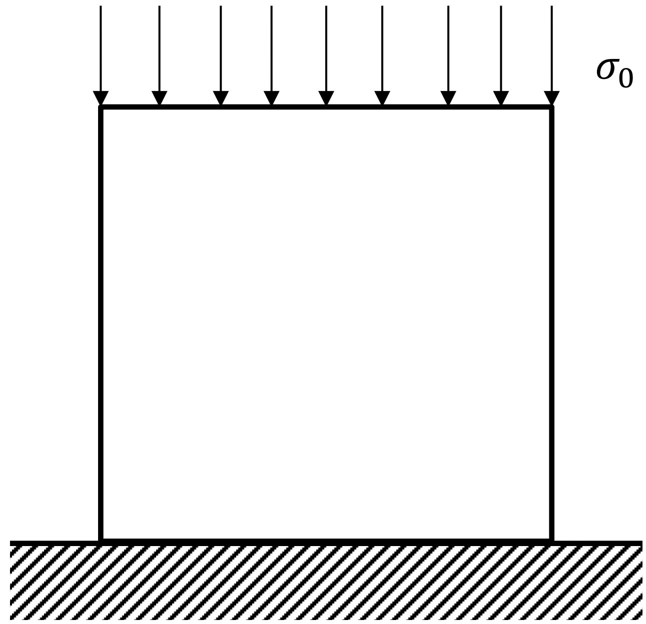

Figure 1-1: The schematic presentation of our proposed food breakdown model. The food particle is modeled as a simplified 2D square and it is under quasi-static loading (σ_0).

1.3.1 Modeling assumptions

- **Two-dimensional plane strain formulation:** The three-dimensional solution for the fracture mechanics problems requires the implementation of computational methods to track the crack surface, which is a computationally expensive task. In this work, the two-dimensional plane-strain formulation is used in order to simplify the complexities of the 3D model. Later in 3.6, the results from the 2D model will be validated against the 3D experimental measurements in order to justify its applicability.
- **Quasi-static compressive loading:** While chewing, the food particles are under compressive loading. In order to prevent any damage to the dentition, the pressure exerted on the food morsels is kept within the quasi-static limits. More details on the quasi-static loading formulation is provided in 3.2.

- **Brittle material properties and LEFM formulation:** Different structures with different material characteristics tend to represent distinct failure behaviors. Therefore, various approaches and criteria were built to envelop these differences. Food materials, in general, can be categorized as brittle or viscoelastic materials. Previous clinical studies have suggested that using brittle materials as test foods for assessing the masticatory performance can provide a more thorough insight into one's chewing ability [11]. Therefore, we focused on the fracture analysis of brittle materials. More details on the effect of food material properties on the mastication will be provided later in 2.4. Linear Elastic Fracture Mechanics (LEFM), the basic theory of fracture analysis, is the suitable formulation for analyzing the fracture behavior of brittle materials (3.3). The present formulation of LEFM have been successfully applied to different classical crack problems. However, for complicated geometries and loading conditions, coupling with a computational tool such as the Finite Element Method (FEM) or meshless methods is required (1.3.2).

1.3.2 Computational methods for fracture analysis: comparison between XFEM and SPH

Application of the conventional FEM to fracture mechanics problems requires extra computational efforts (3.4). This encourages the application of the *Extended Finite Element Method (XFEM)* (3.4.1): an enriched technique that is especially developed to tackle fracture mechanics problems. Besides the grid-based methods, the mesh-free methods have also shown considerable potential to improve the difficulties of using mesh-based methods in solving problems with moving discontinuities [7]. *Smoothed Particle Hydrodynamics (SPH)* (3.4.2), known as a *truly meshless* method, has been applied successfully to problems involving large deformations and discontinuities [8]. Despite all of the advantages of SPH method, its classical formulation demonstrates numerical instability and inaccuracy when subjected to high strain loadings (3.4.2.3). As a result, numerical corrections are required to improve the solution. More details on the suitable SPH formulation and the required numerical corrections are presented in 3.4.2.

Both XFEM and SPH can be regarded as proper candidates for food breakdown modeling. The applicability of the fracture mechanics method to food breakdown modeling is highly dependent on the accuracy of the computational methods. With that being said, a thorough investigation of the strengths and weaknesses of these computational methods is required. This investigation enables us to trace back the sources of error in our final food breakdown model. This means that in order to evaluate the effectiveness of fracture mechanics in food breakdown modeling, a comparison between XFEM and SPH is required. In other words, the comparison is intended to provide an insight on the computational possibilities, rather than finding the most suitable method. The accuracy of XFEM and SPH in solving two-dimensional plane-strain fracture mechanics problems and the sensitivity of their solutions to geometrical factors were assessed using two benchmark tests (3.4.3).

Another major factor to consider while investigating the suitability of a numerical method for simulating the food breakdown is the sensitivity of its solution to variation in the material properties. Later in 3.6, the sensitivity of the SPH fracture model to the variation in the material stiffness and heterogeneity will be investigated. This validated model will then be used in order to simulate a two-dimensional food breakdown model and measure the masticatory performance and the occlusal force (4.2).

1.4 Contributions and thesis outline

The main contributions of this thesis are listed as follows:

- We improved the stability of the classic SPH model for elastic solids under quasi-static compression by using a suitable quadratic function as the smoothing function, applying the NSPH formulation, and identifying the proper coefficients for the artificial stress terms. This improvement was accomplished through a step-by-step analysis of the relevant numerical parameters.
- We modeled a two-dimensional crack using SPH method and provided the formulation for calculating the stress intensity factor. Together with the modified elastic solid formulation, this model provides an improved SPH solution to two-dimensional plane-strain fracture mechanics problems. The stress intensity factor calculated using this model was improved by around 15% compared to the previous works.
- We identified the strengths and weaknesses of XFEM and SPH method in solving two-dimensional fracture mechanics problems. This was done by a thorough comparison between SPH and XFEM in solving two-dimensional fracture benchmark tests, calculating the relevant factors, and assessing the sensitivity of each solution to the variation in the geometrical factors.
- We demonstrated that the SPH method has the potential to simulate the oral food breakdown and to provide accurate measurements for the masticatory performance and the occlusal forces by validating our modified SPH code against the experimental data on brittle materials under compression, and assessing the sensitivity of this method to the variation in the material properties (stiffness and heterogeneity).

- Finally, we demonstrated that a two-dimensional fracture SPH model is capable of measuring the masticatory performance and the occlusal force following one chewing stroke. This suggests that the continuum-mechanics-based food breakdown scheme that is represented in this thesis is a promising method to assess the masticatory performance and the occlusal force, and therefore, it can be considered as an alternative to the current highly-invasive clinical methods. Our model study also represented a strong correlation between the masticatory performance and the food stiffness, which has long been debated in the clinical literature, and yet the experimental approach had failed to properly investigate the correlation. Also, the model study represented a moderate correlation between the masticatory performance and the occlusal force.

This thesis is outlined as follows:

- Chapter 2 reviews the physiology of mastication and the current clinical approaches in quantifying the masticatory ability and the significance of assessing the masticatory performance and the occlusal force correlatively. It also talks about the difficulties associated with clinical data collection and elaborates on the ability of biomechanical modeling in addressing those issues. Finally, it proposes our approach to resolve the issues that were previously mentioned.
- Chapter 3 reviews the fundamentals of the fracture mechanics and formulates our desired two-dimensional LEFM model under quasi-static loading. It presents the different numerical approaches for solving fracture mechanics problems (XFEM and SPH). It analyzes the stability and accuracy of the conventional SPH method and the effects of the numerical modifications on its solution. It also investigates the efficiency of XFEM and

SPH method in solving two-dimensional fracture mechanics problems. Finally, it validates our SPH model against the experimental studies.

- Chapter 4 provides the method for measuring the occlusal force and the algorithm for measuring the masticatory performance using our two-dimensional food breakdown model. Finally, the food breakdown was simulated for a number of brittle food samples to measure the masticatory performance and the occlusal force.
- Chapter 5 summarizes the contributions of this thesis, identifies the strengths and weaknesses of our approach, and discusses the future work.

Chapter 2: Food Breakdown

2.1 Oral food processing

Chewing is a complicated task and its physics is difficult to understand and measure. It involves the coordination between different body parts such as jaw, tongue, cheek, hyoid bone, and masticatory muscles. Fracture mechanics, comminution, particle-particle, food-saliva, and food-oral surface interactions, rheology, and heat and mass transport are mechanisms that transform solid food materials into semifluid and swallowable bolus. Generally speaking, food undergoes comminution, agglomeration, hydration, and dilution phases before being swallowed [9].

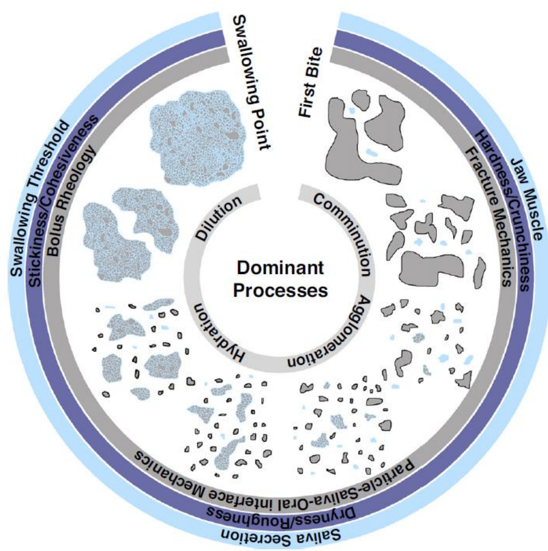

Figure 2-1: As chewing goes on, the food particle size decreases to a minimum desired size. The secretion of saliva makes the particles to swell, soften, and agglomerate before becoming a paste that later dilutes with additional saliva until it reaches the swallowing threshold [9]**.**

Food undergoes four key stages before being swallowed. During the first stage, the ingested food is placed between the teeth to get prepared for breakage. This stage takes about 280 *ms*, which is generally not affected by the food type and its material properties. The second stage, known as the processing phase, is when the food grinding and crushing happens. Material characteristics of food particles affect the time span of this step; it takes longer for harder food materials. As illustrated in Figure 2-2, experimental studies show that the cyclic movement of the jaw in the processing phase is synchronized with the movements of soft palate, tongue, cheek, and hyoid bone [2]. Food's aroma is delivered to chemoreceptors in nose as the jaw and tongue movements pump air into the nasal cavity. As particles are being crushed to the appropriate size during the processing phase, the third stage, also known as the transport stage, gradually begins when smaller food particles move toward the posterior of the oral cavity. Tongue movements manipulate the food particles in order to form a bolus. During the last stage (the pre-swallowing stage), the bolus gets prepared for swallowing by moving toward the posterior of the tongue.

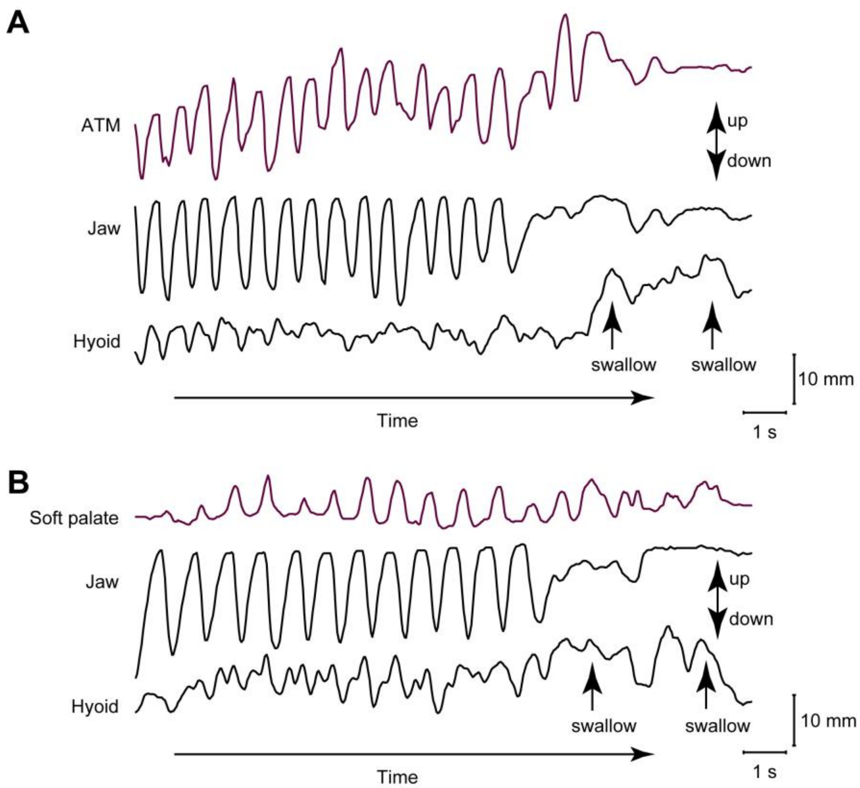

Figure 2-2: A) Movements of the anterior tongue marker (ATM), lower jaw, and hyoid, B) soft palate, jaw, and hyoid bone over time [10]**.**

2.2 Mandibular movements during chewing

The four pairs of masticatory muscles (masseter, temporalis, lateral pterygoid, and medial pterygoid) are responsible for masticatory movements of mandible (Figure 2-3).

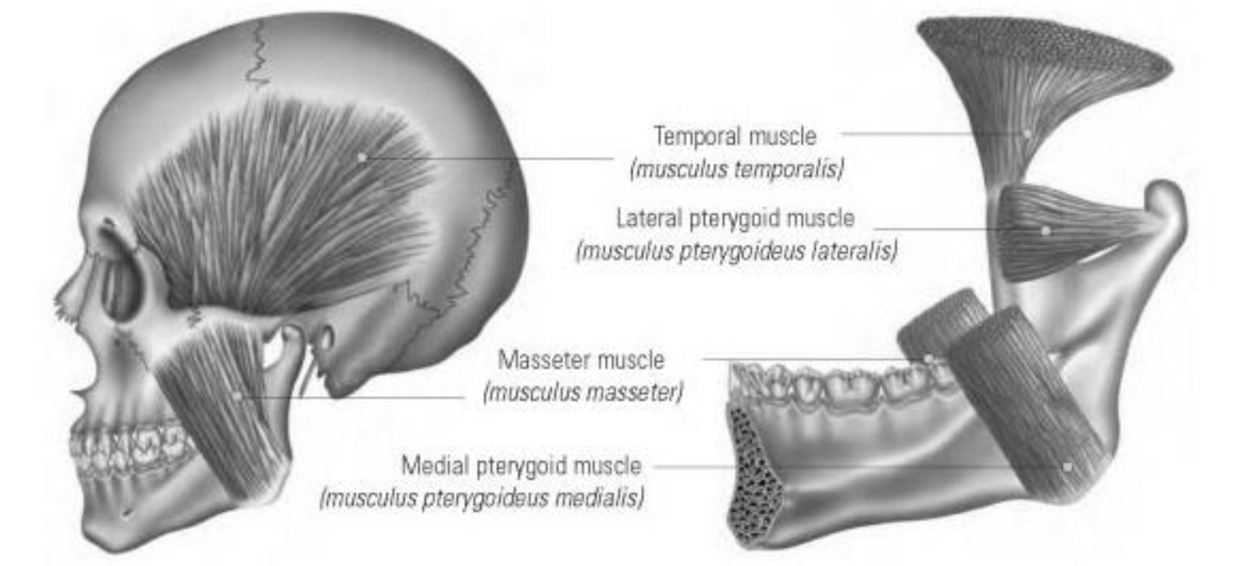

Figure 2-3: Lateral view of the muscles of mastication [11]

Mandibular movements and the neuromuscular control of masticatory muscles have an essential contribution to the chewing process. The efficiency of oral food processing is highly dependent on jaw muscle activity for jaw movements and the required force to cut and comminute the food morsels. Electromyography (EMG) studies on human subjects indicate that a lower level of muscle activity is required during the pseudo-chewing movements without food. Higher level of muscle activity is reported when subjects were asked to chew a food sample (Figure 2-4). This implies that the magnitude of force exerted from jaw muscles is higher during the mastication [2]. During chewing, a small portion of muscular force is used to move jaw in rhythmic pattern and the rest is dedicated to crush food materials.

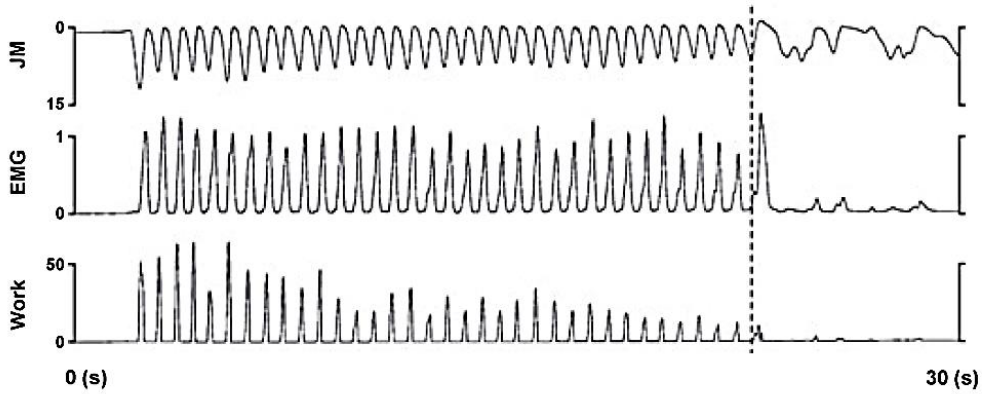

Figure 2-4: From top to bottom, vertical jaw movement (in mm), rectified muscle activity of right and left masseter and temporal muscles (summed) (EMG in mV), and instantaneous muscle work (in $mV.mm.s^{-1}$) of a subject chewing a piece of bread [2]

According to experimental studies, the amount of muscle activity and the resultant bite force varies in different chewing cycles and in foods with different material properties.

2.3 Clinical methods to evaluate the masticatory process

Masticatory function of healthy subjects has been extensively studied in the clinical settings as a standard to evaluate the mastication ability of different patient groups. To facilitate the evaluation process, several clinical methods were created to determine the masticatory efficiency. These methods either target the objective capacity of the masticatory system (*known as the masticatory performance*) or subjectively describe the masticatory satisfaction by investigating the questionnaires filled by the patients.

Several methods have been proposed to determine the *masticatory performance*. These techniques include measuring color change in chewing gum [12], measuring sugar loss from chewing gum [13], measuring the release of dye when chewing raw carrots, photometric methods to evaluate the color change in the chewed food, and optical scanning of food particles [14]. The most commonly used technique is to sieve the comminuted food to evaluate the degree of its breakdown. Natural foods such as carrots, peanuts, and almonds, as well as synthetic materials have been used as the test food in this technique. The test food, masticated for a specified number of cycles, will pass through a sieve with known mesh size. Based on this technique, the masticatory performance is defined as the median particle size of the chewed food. Smaller particle size means better food fragmentation, thus a higher masticatory performance.

Self-assessed masticatory function, commonly known as the masticatory ability, is a subjective metric to evaluate the patients' chewing efficiency. Patients are asked to fill out questionnaires that address their level of satisfaction with oral food comminution, their dental state, and their food pattern selection. Previous studies show that the self-assessed chewing ability does not necessarily correlate with the objective masticatory performance measurements [1]. Although the self-assessed methods are considered as the only means that truly reflects the patient's "perception", laboratory-based quantifications are still required to evaluate the chewing ability.

Another major objective clinical metric to evaluate the masticatory function is the *occlusal force*, defined as the force exerted on opposing teeth when the jaws are closed or tightened. The occlusal force pattern on the human dentition is known to be correlated with the patients' chewing satisfaction [15]; an alteration in the occlusal force amount can cause dissatisfaction with the masticatory process [16]. Therefore, a comprehensive evaluation of masticatory function requires a correlative study of the *masticatory performance* and the *occlusal force*.

2.4 Effects of food material properties on the masticatory measurements

During mastication, the resistance from food particles controls the jaw movements, the activation of masticatory muscles, and the masticatory force. Previous experimental studies have shown that the hardness of food affects the chewing cycle duration and the amplitude of muscle activity; harder foods require higher muscle activity and longer chewing duration to be comminuted properly. In addition, larger jaw movements were reported when the subjects were asked to chew on harder food materials [17].

The occlusal force and the masticatory performance measurements are also affected by the material characteristics of the chewed food (Table 2-1 and Table 2-2).

Food	Force at occlusion (pounds)
Peanuts	78.35
Cheese	50.35

Table 2-1: Occlusal force for hard and soft foods [18]

Food	Mean particle size (mm^2)
Peach	3.28
Mushroom	3.53
Peanut	0.67

Table 2-2: The mean particle size of the chewed food at the swallowing point for different food properties [19]

It is worth mentioning that as the mechanical properties of the natural food materials can vary significantly, the reported values for the masticatory performance and the occlusal force measurements may not be consistent over different experimental studies. Although the previous experimental studies have shown the effect of hardness of the food material on the measurements of the masticatory performance and the occlusal force, the actual correlation between these variables is still not clear. Therefore, the current clinical techniques for evaluation of the masticatory function is not able to accommodate the variability in material properties of the testing foods. This highlights the need for a more inclusive assessment approach.

Previous clinical studies have indicated that the masticatory performance measured from the tests done using brittle materials (peanuts) presents a higher correlation with the other clinical metrics (such as mixing ability) [20]. This suggests that compared to visco-elastic food materials, using brittle materials as test foods can provide a more comprehensive insight into one's masticatory ability.

2.5 Computational models of food comminution

Computational modeling of food breakdown has the ability to bridge the gap between food structural properties and the human masticatory system. A thorough model of oral food breakdown not only is a great tool to understand the masticatory system, but also can be utilized in food industry to examine the quality of food products. Three-dimensional finite-element models of mandible and muscles of mastication have been created in the previous studies [21][22] in order to simulate the jaw dynamics and to study the muscle forces acting on the jaw and to evaluate the stresses applied on the teeth and the jaw bone. Food breakdown modeling, on the other hand, has not received the same amount of attention.

Different approaches have been adopted to model oral food breakdown. Voon et al. (1986) [23] employed a method, previously proposed to analyze the comminution systems, to investigate the probability of a food particle being crushed. Based on previous empirical observations on mastication and oral food breakdown patterns, they introduced two power functions, selection and breakage functions, that predict the distribution of the food particles at a given particle size after a number of chewing cycles. Although this approach can evaluate the masticatory performance, it is not able to associate the masticatory performance and the occlusal force in order to provide a comprehensive insight into the masticatory function. In addition, the empirical nature of these proposed functions limits the applicability of this method to particular material properties and dentition status, due to the testing restrictions.

Sun and Xu (2008) [24] used Discrete Element Method (DEM) to model food breakdown during mastication and material transport during swallowing. The primary goal of this work was to present a novel application of DEM. However, they did not present any quantitative measurements of their results and did not validate them against the experimental data. This questions the applicability of DEM to the oral food comminution modeling.

The alternative approach to computationally represent the oral food breakdown is using the continuum-mechanics-based models. Applying the fundamentals of fracture mechanics and elastic solid deformation, these models are able to predict the force required to breakdown a food morsel and to track the crack propagation process, giving them the potential to associate masticatory performance and occlusal forces in order to build a thorough representation of oral food breakdown.

Harrison et al. (2014) [6] used Smoothed Particle Hydrodynamics (SPH) method to inspect the food comminution. They proposed a SPH-biomechanical model of oral cavity in order to study the aroma release and taste perception. A three-dimensional model of food was coupled to a three-dimensional biomechanical model of teeth and tongue in order to take the interaction between food and oral cavity into consideration, and as a result, to represent a realistic food comminution model. This study was mostly focused on food engineering applications and less attention was dedicated to evaluate the masticatory ability.

With all these in mind, in this thesis, we are going to build a two-dimensional continuum-mechanics based model of food breakdown which is capable of measuring the masticatory performance and the occlusal force, following one chewing stroke. Besides assessing the masticatory function, this modeling approach associates the main components of the masticatory system and fills the gap in the previous biomechanical models of mastication.

On the next chapter, the fundamentals of fracture mechanics and the relevant computational methods to solve a two-dimensional brittle fracture problem will be discussed.

Chapter 3: Fracture Mechanics

3.1 Introduction

The term “fracture” describes the local detachment of material cohesion in a solid body. Fracture mechanics is a field that studies the process that either leads to partial disruptions and development of incipient cracks or causes an entire breakdown and failure of a mechanical structure. In other words, it analyzes the relationship among stresses, cracks, and fracture toughness. Fundamental aspects of the theory of the fracture mechanics were created based on the experimental observations and the theoretical elasticity.

Before presenting the appropriate fracture mechanics formulation, it is important to review the modeling assumptions. These assumptions were made based on the physics of mastication and the characteristics of our desired food breakdown model.

3.2 Modeling assumptions

Due to the fact that fracture and structural failure can happen under various conditions, fracture processes are categorized based on different individual aspects. The most common way to classify the fracture processes is based on type of external loading and material characteristics.

Mechanical loads are divided into static, dynamic, and variable (cyclic) loads based on their temporal progress. While chewing the food, to avoid any damage to the teeth and the masticatory system, the applied force on the food material is slowly increased to a maximum value. This suggests that the oral food breakdown can be modeled as a quasi-static process, where the inertial forces and dynamics effects can be neglected.

Different materials, depending on the amount of plastic deformation that they macroscopically experience before being fractured, fall into two major classes: *brittle* and ductile.

Experimental studies have shown that brittle materials tend to fracture without any significant plastic deformation, when subjected to a critical stress value [25]. The load-deformation diagram runs linearly before reaching a critical point where the crack propagation begins (Figure 3-1). It is generally accepted that the strength of a material to resist fracture is its inherent property. In ductile materials on the other hand, extensive plastic deformation occurs before fracture. The plastic zone outspreads over the entire cross section and the load-deformation diagram represent a distinctive non-linearity.

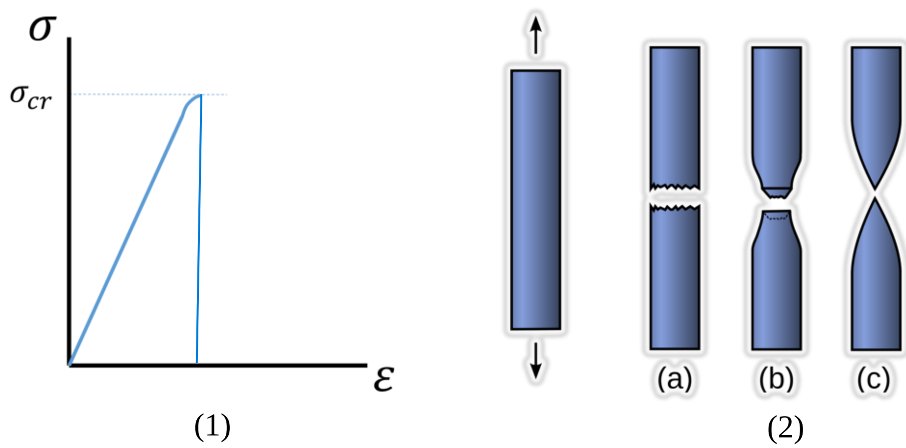

Figure 3-1: 1) Load-deformation diagram for a brittle material, 2) plastic zone in a: brittle, b: quasi brittle, and c: ductile materials

In this work, as described in 2.3, we are trying to imitate the clinical tests for masticatory performance; therefore, the main focus is put on the fracture modeling of brittle materials.

In summary, our focus in this work will be on the fracture analysis of the brittle materials under quasi-static loading. In order to properly represent this fracture process, linear elastic fracture mechanics (LEFM) formulation is going to be applied to our fracture model. More details on LEFM is provided in 3.3.

3.3 Linear elastic fracture mechanics (LEFM)

In order to mathematically represent different fracture processes, distinctive disciplines have been created. Linear elastic fracture mechanics (LEFM) assumes that the mechanical body is made of ideally linear-elastic and isotropic material and that it represents an insignificant plastic deformation. This makes LEFM the appropriate framework to investigate the fracture process in brittle materials.

In fracture mechanics, crack propagation is analyzed using three independent crack modes: Mode-I (opening), Mode II (sliding), and Mode III (tearing). Fractures can be described based on one or a combination of these modes. In a two dimensional model, only Figure 3-2(a) and Figure 3-2(b) happens.

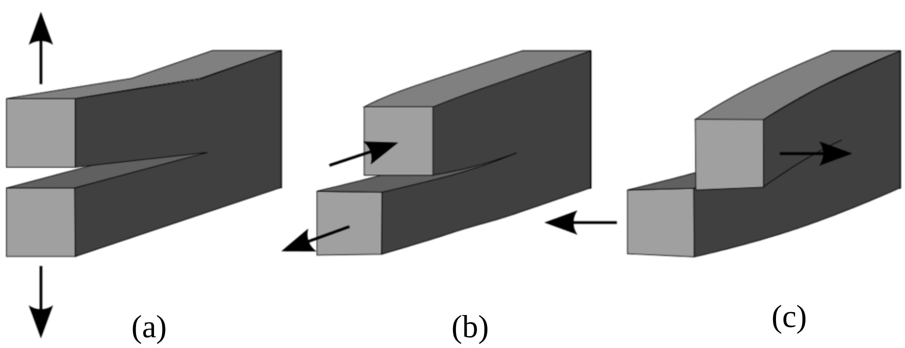

Figure 3-2: Different fracture modes, a) opening, b) sliding, c) tearing

In the classical theory of strength of materials, it is common to consider mechanical components as ideally flawless bodies and the maximum allowable applied stress as the material yield stress. However, experimental studies indicate that the crack propagation initiates from the existing cracks and flaws that are usually created during the manufacturing process. This constitutes one of the primary assumptions in fracture mechanics analysis. The classical theory of elasticity solution for an infinite plate containing a sharp central crack, predicts an infinite stress [26] value at the tip of the crack. However, it is known that no material can tolerate an infinite amount of stress state. Therefore, fracture mechanics advises a local stress intensity factor (SIF or *K* factor) or a global fracture energy release rate (G) to analyze the fracture occurrence. The measured *K* or G will then be compared to their critical values as an alternative failure criterion.

3.3.1 Stress intensity factor, *K*

Stress intensity factor was introduced by *Irwin* (1957) as a measure for the strength of singularity. He proposed that all elastic stress fields are distributed in a similar way and *K* controls the local stress quantity.

Based on Irwin's work, the stress state around a crack tip in a general form can be represented as (3-1):

$$\sigma_{ij} = r^{-\frac{1}{2}}\left\{K_I f_{ij}^{I}(\theta) + K_{II} f_{ij}^{II}(\theta) + K_{III} f_{ij}^{III}(\theta)\right\} + higher\ order\ terms \tag{3-1}$$

where σ_{ij} are the near crack tip stresses, K_I, K_{II}, and K_{III} represent the intensity factors associated with three independent crack modes, and *r* and θ represent the polar coordinates around the crack tip.

$$K_I = \lim_{\substack{r\to 0\\ \theta=0}} \sigma_{yy}\sqrt{2\pi r} \tag{3-2}$$

$$K_{II} = \lim_{\substack{r\to 0\\ \theta=0}} \sigma_{xy}\sqrt{2\pi r} \tag{3-3}$$

$$K_{III} = \lim_{\substack{r\to 0\\ \theta=0}} \sigma_{yz}\sqrt{2\pi r} \tag{3-4}$$

Mode I intensity factor can be written as:

$$K_I = \lim_{\substack{r \to 0 \\ \theta = 0}} \sigma_{yy}\sqrt{2\pi r} = \lim_{\substack{r \to 0 \\ \theta = 0}} \sqrt{2\pi r}\sigma_0\sqrt{\frac{a}{2r}}\cos\frac{\theta}{2}\left(1 - \sin\frac{\theta}{2}\sin\frac{3\theta}{2}\right) = \sigma_0\sqrt{\pi a} \tag{3-5}$$

The critical value of the stress intensity factor K_{ic}, is called fracture toughness and represents the ability of a material to resist the progressive tensile crack extension.

The stress tensor (in polar coordinate, mode I loading) can be written as (3-6):

$$\begin{Bmatrix} \sigma_{xx} \\ \sigma_{yy} \\ \sigma_{xy} \end{Bmatrix} = \frac{K_I}{\sqrt{2\pi r}} \begin{Bmatrix} \cos\frac{\theta}{2}\left(1 - \sin\frac{\theta}{2}\sin\frac{3\theta}{2}\right) \\ \cos\frac{\theta}{2}\left(1 + \sin\frac{\theta}{2}\sin\frac{3\theta}{2}\right) \\ \sin\frac{\theta}{2}\cos\frac{\theta}{2}\cos\frac{3\theta}{2} \end{Bmatrix} \tag{3-6}$$

$$\sigma_{zz} = \begin{cases} \nu\left(\sigma_{xx} + \sigma_{yy}\right) & plane\ strain \\ 0 & plane\ stress \end{cases} \tag{3-7}$$

$$\sigma_{xz}, \sigma_{yz} = 0 \tag{3-8}$$

3.3.2 Griffith's energy release theory and its relationship with K factor

Griffith (1921) [27] observed an inconsistency between the experimental and the theoretical tensile strength of solids. In order to reconcile these contradictory facts, he proposed a thermodynamics-based failure criterion to be utilized instead of the previous stress-based criterion.

For an isotropic, ideally brittle material, under quasi-static loading, the Griffith crack growth energy (G) can be written as (3-9):

$$G = -\frac{\partial \Pi}{\partial a} = 2\gamma_s \tag{3-9}$$

where Π is the potential energy, *a* is the crack half length, and γ_s is the surface energy. The factor 2 represents the existence of two material surfaces upon fracture. (3-9) indicates that based on the first law of thermodynamics, the decreasing rate of potential energy is equal to the surface energy dissipated during the crack growth. Crack propagation happens when the energy release rate per crack extension is greater than the surface energy:

$$-\frac{\partial \Pi}{\partial a} \geq 2\gamma_s \tag{3-10}$$

Based on the energy equations, the critical stress can be written as:

$$\sigma_{cr} = \sqrt{\frac{2E'\gamma_s}{\pi a}} \tag{3-11}$$

where *E'*=*E* (plane stress) and *E'*=$\frac{E}{1-\upsilon^2}$ (plane strain). The critical stress intensity factor K_C is defined as (3-12):

$$K_C = \sigma_{cr}\sqrt{\pi a} \tag{3-12}$$

For mixed mode I and mode II problem, the relationship between G and K_I and K_{II} is written as (3-13):

$$G = \frac{K_I^2 + K_{II}^2}{E'} \tag{3-13}$$

3.3.3 Solution procedure for *K* and *G*

In this work, a direct method for evaluation of stress intensity factor is used. By finding the difference in the total strain energy for initial crack length a and extended crack of length $a + \Delta a$, using the direct definition ($G = -\frac{\Delta \Pi}{\Delta a}$), *G* can be calculated. For a purely mode-I problem:

$$G_1 = \frac{K_I^2}{E'} \tag{3-14}$$

Using (3-14), the mode-I stress intensity factor will be identified.

For mixed-mode fracture problems, G_1 is calculated by extending the crack length by Δa in the direction of $\theta = 0$, and G_2 is calculated by extending the crack in the direction of $\theta = \pi/2$. Mode-I and mode-II stress intensity factors are then calculated using (3-14) and (3-15):

$$G_2 = \frac{-2K_I K_{II}}{E'} \tag{3-15}$$

3.4 Numerical methods for fracture analysis

Analytical solutions are usually not available for the real-world problems due to the geometrical complications. Alternatively, numerical techniques such as the FEM or the meshless family of methods are employed to provide an approximation to the exact solution.

Finite Element Method (FEM) has been utilized successfully in many applications. However, due to the mesh-based nature of this method, low quality or distorted meshes can cause inaccuracy. Particularly speaking, the conventional FEM does not allow the cracks to cut through the elements; crack propagation line has to align with the element edges. This issue is usually resolved by performing remeshing algorithms around the crack tip. These algorithms are computationally expensive, impracticable to run on complicated geometries, and require transforming the calculated quantities to the newly created meshes and as a result, a possible degradation of accuracy.

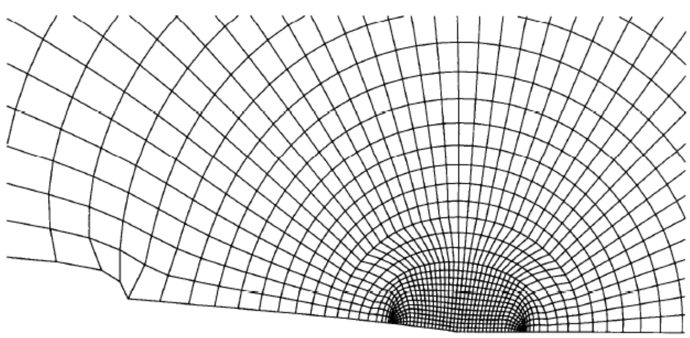

Figure 3-3: High-resolution FE mesh around the crack tip

In order to overcome the problems associated with the classical FEM solution to fracture mechanics, enriched numerical techniques such as the Extended Finite Element method (XFEM) were developed.

Theoretically, the main goal of enrichment is to increase the order of completeness of the approximation functions; enriched functions can capture the analytical solution more accurately. Computationally speaking, it incorporates the information obtained from the analytical solution into the approximation in order to reach a higher accuracy. The choice of the enriched functions depends on the *a priori* solution of the problem.

There are two main approaches to enrich the approximation function: *intrinsic*, and *extrinsic* enrichment. The intrinsic approach increases the order of the completeness of the shape functions directly, whereas the extrinsic approach enriches the approximation by integrating additional shape functions into it. Several numerical methods have been developed based on each of these two approaches. In this work, we are going to focus on the smoothed particle hydrodynamics (SPH) method as a numerical technique that is based on the intrinsic enrichment scheme, and on the extended finite element method as the one with the extrinsic enrichment approach. These two numerical methods were implemented in MATLAB and were applied to a simple two-dimensional crack propagation problem. The advantages and disadvantages of each method will be investigated later in 3.4.3.

3.4.1 Extended finite element method (XFEM)

The most recent version of XFEM, developed by Dolbow et al. (2000) [28], is a generalization to the conventional FEM that presents a technique to model discontinuities in the FE framework by locally enriching the approximation based on the partition of unity method (PUM) [29].

For point x, belonging to an arbitrary domain discretized into n nodes, the approximation for the field variable u (displacement) in the FE scheme is written as (3-16):

$$u(x) = \sum_{j=1}^{m} N_j(x) u_j \tag{3-16}$$

where N_j is the matrix of shape functions and u_j is the matrix of nodal displacement. Based on the partition of unity theory, XFEM proposed a scheme that enables the nodes belonging to the discontinuity (crack) domain to represent an additional degree of freedom by locally enriching the approximation space. Basic XFEM approximation for an isotropic material is written as (3-17):

$$u^h(x) = u^{FE} + u^{enr} = \sum_{j=1}^{m} N_j(x) u_j + \sum_{k=1}^{n} N_k(x) \psi(x) a_k \tag{3-17}$$

where u_j is the matrix of regular nodal degrees of freedom, a_k is the additional set of degrees of freedom to the standard FE model and $\psi(x)$ is the discontinuous enrichment function that is applied to the set of nodes which are influenced by the discontinuity domain. As it is evident from (3-17), the enrichment is fulfilled by extrinsically integrating additional terms to the main approximation scheme, implying that XFEM falls into the extrinsic enrichment category.

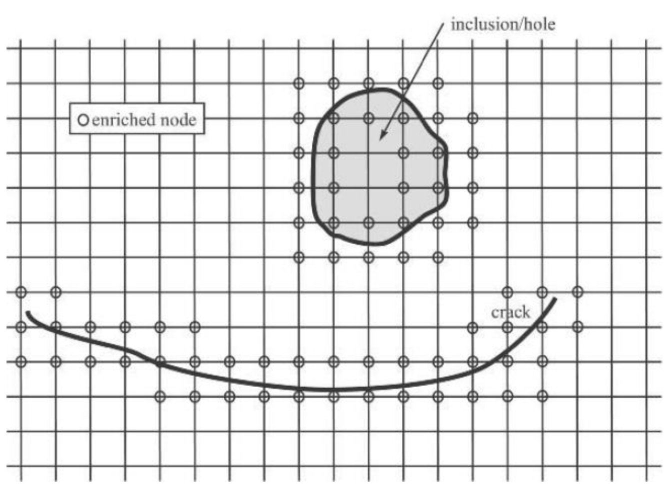

Figure 3-4: Enrichment support domain

The enrichment function of $\psi(x)$ is chosen by considering the appropriate analytical solution according to the type of discontinuity. On top of that, the enrichment function is required to reproduce singular stress field around the crack tip, satisfy the continuity condition across the adjacent finite elements, and to provide distinct strain fields across the crack line. Keeping all of these objectives in mind, the enrichment function (in polar coordinates) can be defined as (3-18):

$$\{\psi(x)\} = \left\{\sqrt{r}sin\frac{\theta}{2}, \sqrt{r}cos\frac{\theta}{2}, \sqrt{r}sin\frac{\theta}{2}sin\theta, \sqrt{r}cos\frac{\theta}{2}sin\theta\right\} \tag{3-18}$$

3.4.2 Smoothed particle hydrodynamics (SPH)

Originally proposed by Monaghan et al. (1977) [30] for use in solving astronomical gas dynamic problems, smoothed particle hydrodynamics (SPH) is one of the oldest truly meshless or particle-based numerical methods utilized to approximate the solution to the PDE systems. The main idea behind this method is to discretize the computational domain into SPH particles and approximate the field variable for each of these particles using a suitable kernel function (smoothed kernel function).

For an arbitrary function *f*, the discretized format of SPH approximation ($< f >$) can be written as:

$$< f(x) > = \sum_I^N \frac{m_I}{\rho_I} W(x - x_I, h) f_I \tag{3-19}$$

where m_I is the mass and ρ_I is the density of particle I, and the summation covers all the particles I that are located within a radius *h* of point *x*. The smoothing kernel $W(x - x_I, h)$ has its maximum value at point *x* and has compact support with radius 2h (Figure 3-5). More details on how to select the appropriate kernel function and its influence on the accuracy and the stability of SPH model will be presented in 3.4.2.3.

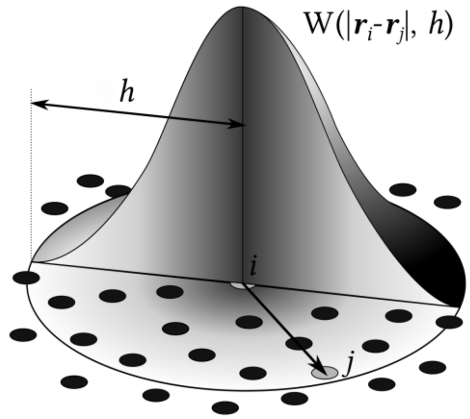

Figure 3-5: Smoothing function

By differentiating (3-19), the gradient of function $f(x)$ is given as:

$$< \nabla f(x) > = \sum_I^N \frac{m_I}{\rho_I} \nabla W(x - x_I, h) f_I \tag{3-20}$$

As it is observable from (3-20), the enrichment is done intrinsically using the kernel function and therefore, SPH can be regarded as an intrinsic enrichment method.

SPH method has been widely applied to fluid dynamics problems, especially complex flow simulations, fluid-solid interactions, and multi-physics applications. In addition, the grid-free feature of SPH avoids the difficulties associated with mesh distortion and sustaining mesh integrity; therefore, it is considered as a suitable numerical tool for problems involving large deformations and discontinuities, such as fracture mechanics, and fragmentation [8].

3.4.2.1 Constitutive model

Libersky and Petschek (1990) [31] were the first to extend the SPH method to solid mechanics and strength of materials problems. Applying the SPH approximation scheme to solid mechanics formulation, the governing equations for a two-dimensional solid body, under plane-strain assumption, can be formulized as the following equations:

$$\frac{dx_\alpha^i}{dt} = v_a^i \tag{3-21}$$

Satisfying the conservation of mass (continuity equation):

$$\frac{d\rho_i}{dt} = \sum_j m_j (v_\beta^i - v_\beta^j) \frac{\partial W_{ij}}{\partial x_\beta} \tag{3-22}$$

The elastic deformation calculated using the momentum equation:

$$\frac{dv_\alpha^i}{dt} = \sum_j m_j (\frac{\sigma_{\alpha\beta}^i + \sigma_{\alpha\beta}^j}{\rho_i \rho_j}) \frac{\partial W_{ij}}{\partial x_\beta} \tag{3-23}$$

Hooke’s law for a two-dimensional, plane-strain, elastic body:

$$\frac{d\sigma_{\alpha\beta}^i}{dt} = \frac{E}{(1+\nu)(1-2\nu)} ((1 - \nu\dot{\epsilon}_{\alpha\beta}^i + \nu\dot{\epsilon}_{kk}^i \delta_{\alpha\beta}) \tag{3-24}$$

Strain-displacement relation for a two-dimensional, plane strain problem:

$$\dot{\epsilon}_{\alpha\beta}^i = \frac{1}{2} (\frac{dv_\alpha^i}{dx_\beta} + \frac{dv_\beta^i}{dx_\alpha}) \tag{3-25}$$

Discretizing the velocity derivatives:

$$\frac{dv_\alpha^i}{dx_\beta} = \sum_j m_j (v_\alpha^j - v_\alpha^i) \frac{\partial W_{ij}}{\partial x_\beta} \frac{m_j}{\rho_j} \tag{3-26}$$

It is worth noting that there are several variations of the constitutive equations applied to a SPH model ((3-22)-(3-26)). Although all these variations have the similar physical significance, they may not provide the same level of accuracy at the end. The format presented here has been proven as the most promising version for use in the fracture mechanics applications [32].

3.4.2.2 Time integration

SPH algorithm converts the original continuum partial differential equations into sets of ordinary differential equations; therefore, any stable time-stepping technique that is used for solving ODEs is applicable.

A modified version of explicit, leapfrog time integration is used in this work [33]:

$$v_{n+1/2} = v_{n-1/2} + (\frac{dv}{dt})_n \Delta t \tag{3-27}$$

$$\rho_{n+1/2} = \rho_{n-1/2} + (\frac{d\rho}{dt})_n \Delta t \tag{3-28}$$

$$\sigma^{\alpha\beta}_{n+1/2} = \sigma^{\alpha\beta}_{n+1/2} + (\frac{d\sigma^{\alpha\beta}}{dt})_n \Delta t \tag{3-29}$$

$$x_{n+1} = x_{n-1} + v_{n+1/2} \Delta t \tag{3-30}$$

The Courant-Friedrichs-Lewy (CFL) condition, requires the time steps to be set according to the smallest spatial resolution, the smoothing length *(h)* in this case. Therefore, in order to achieve numerical convergence:

$$\Delta t = \min(\frac{h}{c}) \tag{3-31}$$

where c is the speed of sound in the studied medium.

3.4.2.3 Stability analysis

The classical SPH method suffers from numerical inefficiencies referred to as tensile and compression instability, leading to particles clumping together or a sudden large displacement of particles, and consequently, an erroneous numerical fracture (Figure 3-6). It was commonly believed that instability happens for solid bodies under tension and not for those in compression. However, detailed numerical studies have shown that applying an unsuitable kernel function can cause compression instability as well [34]. Here, first we are going to choose a proper kernel function and evaluate how it affects the stability of our numerical analysis, and after that, we are going to review the available correction methods and investigate the ones that best suits our application.

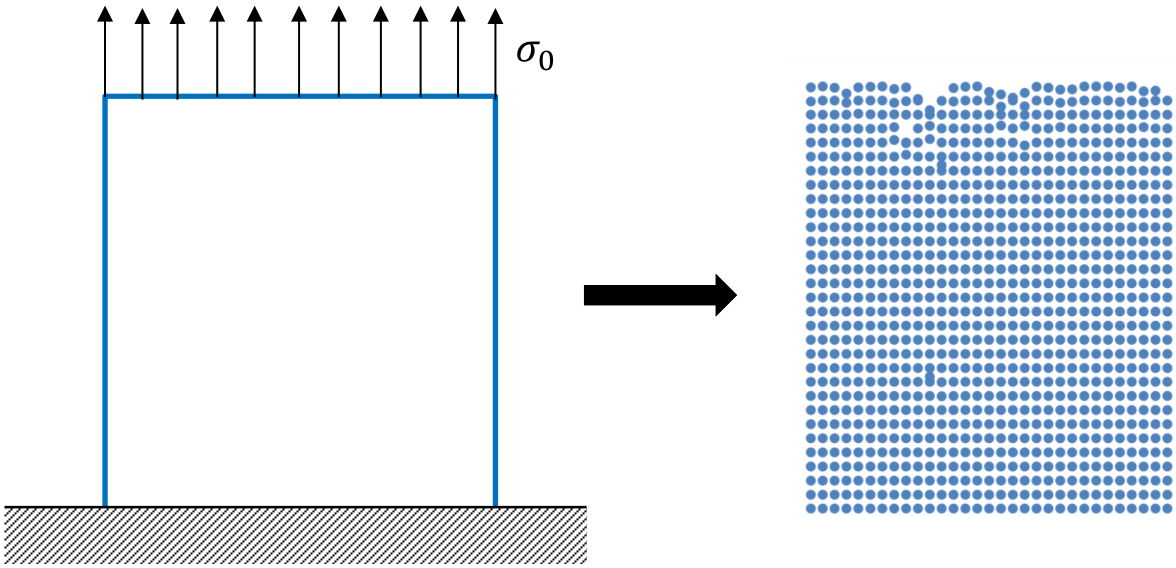

Figure 3-6: Tensile instability: particle clump and boundary deficiency in the conventional SPH

Instability condition

The so-called instability does not depend on the time integration algorithm and there is no stress threshold for its outset. The stability analysis done by Swegle et al. (1995) [34] indicates that for a one-dimensional model, the instability grows under the condition presented as (3-32):

$$\left(\frac{\partial^2 W}{\partial x^2}\right)\sigma_{xx} > 0 \tag{3-32}$$

Taking compressive stress as a negative and tensile stress as a positive number, the instability happens when *W''*<0 for bodies under compression, and when *W*''> 0 under tension.

Smoothing function

The most commonly used smoothing function in solid mechanics SPH models, the cubic B-spline, can be written as:

$$\begin{cases} W_{ij} = \frac{1}{\pi h_{ij}^2}\left[\frac{15}{7}\left(\frac{2}{3} - q_{ij}^2 + \frac{1}{2} q_{ij}^3\right)\right], & 0 \le q_{ij} \le 1 \\ W_{ij} = \frac{1}{\pi h_{ij}^2}\left[\frac{5}{14}\left(2 - q_{ij}\right)^3\right], & 1 \le q_{ij} \le 2 \\ 0\,, & 2 \le q_{ij} \end{cases} \tag{3-33}$$

where $q_{ij} = \frac{r_{ij}}{h_{ij}}$ and h_{ij} is the smoothing length. As it is evident from Figure 3-7, the second derivative of this function (*W''*) is positive for $r > \frac{2}{3}$, leading to tensile instability.

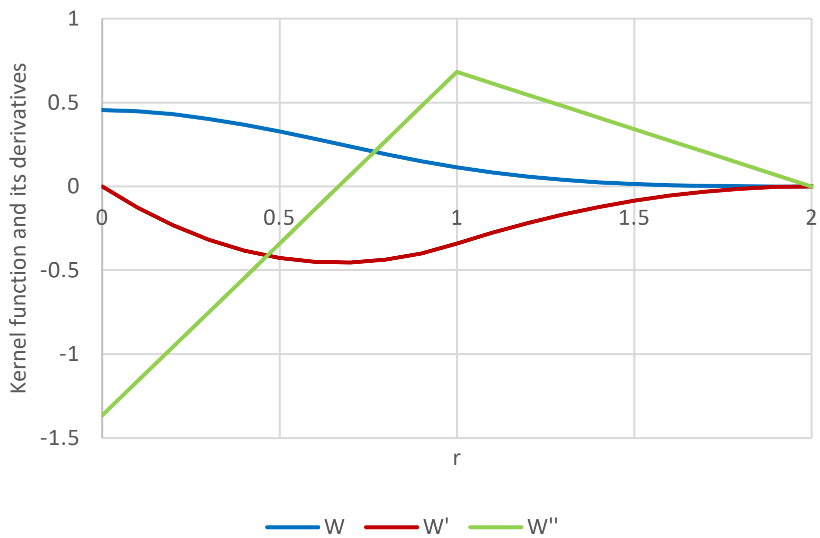

Figure 3-7: Cubic B-spline kernel function and its first and second derivatives

Besides investigating the *W*'', (3-23) and (3-26) show that it is the first derivative of smoothing function (*W*') that acts as the weighting function for the strain rates and forces. From Figure 3-7, it is observable that *W*' reaches its minimum value at $r = \frac{2}{3}$ (maximum for -*W*'). The weighting functions (-*W*' in this case) is expected to continuously decrease as we move away from the center node. Violating this criterion can cause instabilities in compression.

The drawbacks that were mentioned disqualify the cubic B-spline function presented in (3-33) as an appropriate smoothing function. As an alternative, a quadratic smoothing function, written as (3-34), is used in this work:

$$W_{ij} = \frac{1}{\pi h_{ij}^2}\left[\frac{3}{8}q_{ij}^2 - \frac{3}{2}q_{ij} + \frac{3}{2}\right], \quad 0 \le q_{ij} \le 2 \tag{3-34}$$

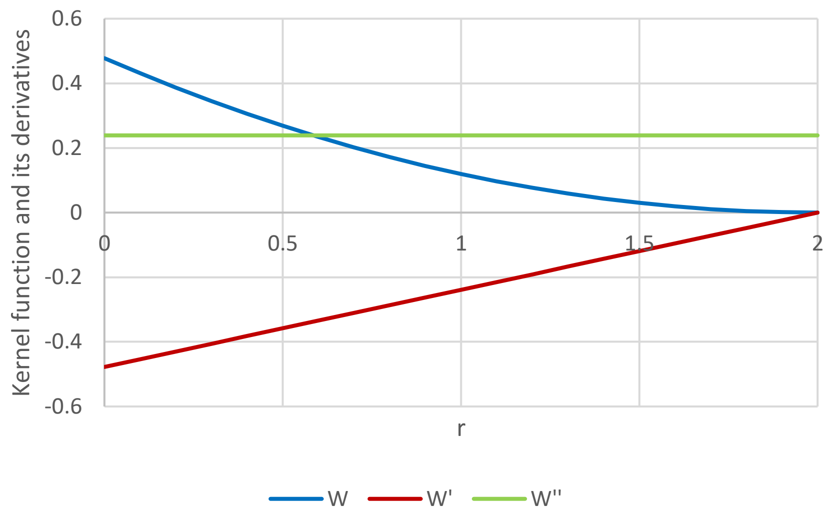

Figure 3-8: Quadratic kernel function and its derivatives

As seen in Figure 3-8, -*W*' decreases as *r* reaches the outer nodes and the compression instability is avoided since *W''* is positive over the entire domain. Although the compression instability is solved, the tensile instability still happens, implying that the tensile and compressive instability cannot be solved together at once [35]. The classical formulation of SPH needs to be modified in order to resolve this problem.

Normalized smoothed particle hydrodynamics (NSPH) method

The modified versions of SPH method can be classified into two family of techniques: *Stress points SPH* and *Normalized SPH.*

Introduced by Dyka and Ingel [36], the stress points SPH uses two sets of particles (master particles and slave particles) to run the numerical analysis. The master particles are the actual SPH particles (also called the velocity particles) and are used to evaluate the kinematic variables (velocity, acceleration, etc.). The slave particles (stress points) are used to calculate the stresses and internal forces. Although this method improves the accuracy and stability of simple one-dimensional SPH models, its application to complicated multi-dimensional bodies can be problematic [37]. Creating the slave particles at the correct position and maintaining the relative positions of them to the master particles is a computationally difficult task to perform, especially for the geometries undergoing large deformations.

Another technique to resolve the issues associated with the classical SPH is called the Normalized SPH. The main idea behind NSPH is to provide the exact strain rates in principal directions for states of constant strain rates (linear velocity distribution). In order to achieve this, the kernel function should be rewritten as [38]:

$$f_i = \frac{\sum_{j=1}^{N} m_j f_j W_{ij}/\rho_j}{\sum_{j=1}^{N} m_j W_{ij}/\rho_j} \tag{3-35}$$

(3-35) is the basic formulae of NSPH and will be applied to (3-22)-(3-26) to solve our model.

A solid body, represented by 25 SPH particles, is subjected to the strain rate $\dot{\varepsilon} = 1$. Figure 3-9(a), shows the equivalent strain rates calculated on each of the particles using the original SPH formulation, and in Figure 3-9(b), the strain rates calculated using NSPH are presented. As seen in Figure 3-9(a), the original SPH method underestimates the strain rate values for the particles on boundary and on the corner which causes instability and boundary deficiency. After switching to the NSPH formulation Figure 3-9(b), strain rates are calculated more accurately and as a result, the discussed boundary deficiencies are resolved.

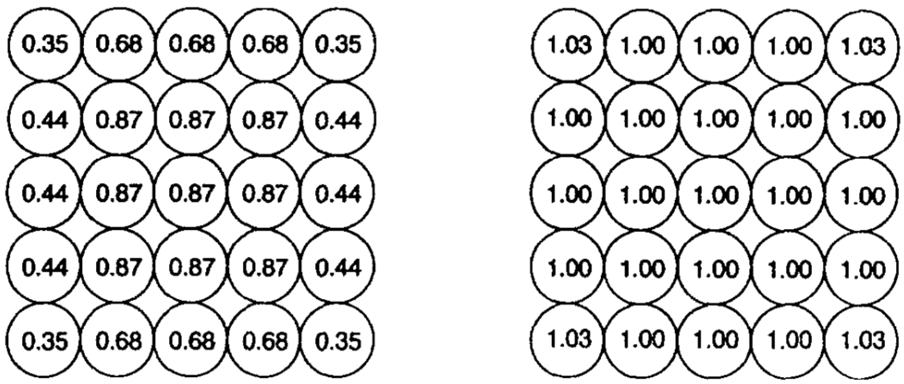

(a) (b)

Figure 3-9: Strain rates calculated using a) classical SPH method and b) Normalized SPH [35]

As an example, a two-dimensional bending cantilever beam is presented in Figure 3-10. The 0.5m in 6m rod was modeled using 1331 uniform particles. The particles at the top and at the bottom are fixed and a compressive force is applied to the middle of the rod. Figure 3-10(a) shows the deformed shape of the beam, simulated using the NSPH, and Figure 3-10(b) is simulated using the classical formulation of SPH. Due to the numerical instability associated with the classical SPH (Figure 3-10(c)) particles at the boundary tend to clump together (boundary deficiency), which causes singularity and forces the simulation to terminate. The 2D bending test represented in Figure 3-10 shows that by switching to NSPH formulation, the boundary deficiencies are resolved.

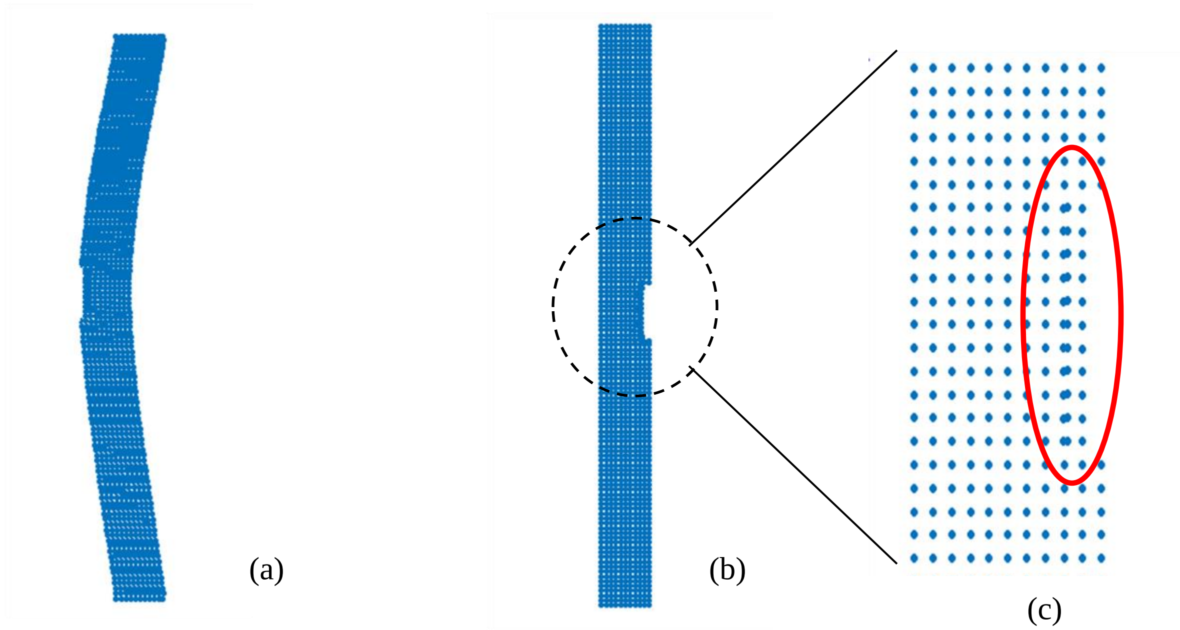

Figure 3-10: A two-dimensional bending beam simulated using a) NSPH b) classical SPH. The instable region is magnified in (c). The boundary particles inside the red curve are clumped together which causes instability.

Numerical oscillation and artificial viscosity

Due to the presence of shocks and discontinuities in the early stages of simulation and the inability of SPH to dissipate them, significant numerical fluctuations are usually observed in the SPH solution. In order to resolve these unphysical oscillations, it is common to add artificial viscosity and artificial stress terms to the momentum equation. Therefore, (3-23) is rewritten as:

$$\frac{dv_\alpha^i}{dt} = \sum_j m_j \left(\frac{\sigma_{\alpha\beta}^i + \sigma_{\alpha\beta}^j}{\rho_i \rho_j} + \Pi_{ab} I + (R_i^{\alpha\beta} + R_j^{\alpha\beta}) f_{\alpha\beta}^n\right) \frac{\partial W_{ij}}{\partial x_\beta} \quad (3\text{-}36)$$

where R_i and R_j are the artificial stress tensors of particle *i* and *j* (calculated from (3-37)-(3-45)), $f_{ij} = W_{ij}/W(\Delta d, h)$, and *n* (the exponent in $f_{\alpha\beta}^n$**)** is an index that ensures the effect of the artificial stress is limited to the neighboring particles. For a two-dimensional problem, the artificial stress components can be calculated using (3-37)-(3-45) [39]:

$$R_i^{xx} = R'^{xx}_i cos^2\theta_i + R'^{yy}_i sin^2\theta_i \tag{3-37}$$

$$R_i^{yy} = R'^{xx}_i sin^2\theta_i + R'^{yy}_i cos^2\theta_i \tag{3-38}$$

$$R_i^{xy} = (R'^{xx}_i - R'^{yy}_i) sin\theta_i cos\theta_i \tag{3-39}$$

$$tan2\theta_i = \frac{2\sigma_i^{xy}}{\sigma_i^{xx} - \sigma_i^{yy}} \tag{3-40}$$

$$R'^{xx}_i = \begin{cases} -\varepsilon \frac{\sigma'^{xx}_i}{\rho_i^2} & \sigma'^{xx}_i > 0 \\ 0 & otherwise \end{cases} \tag{3-41}$$

$$\sigma_i^{xx} = \sigma'^{xx}_i cos^2\theta_i + \sigma'^{yy}_i sin^2\theta_i + 2cos\theta_i sin\theta_i \sigma'^{xy}_i \tag{3-42}$$

$$\sigma_i^{yy} = \sigma'^{xx}_i sin^2\theta_i + \sigma'^{yy}_i cos^2\theta_i - 2cos\theta_i sin\theta_i \sigma'^{xy}_i \tag{3-43}$$

The artificial viscosity, Π_{ab}, is written as:

$$\Pi_{ab} = \begin{cases} \frac{\alpha c \eta_{ab} + \beta \eta_{ab}^2}{\bar{\rho}_{ab}} & (v_a - v_b).(r_a - r_b) < 0 \\ 0 & (v_a - v_b).(r_a - r_b) \geq 0 \end{cases} \tag{3-44}$$

where

$$\eta_{ab} = \frac{h(v_a - v_b).(r_a - r_b)}{|r_a - r_b|^2} \quad and \quad \bar{\rho}_{ab} = \frac{\rho_a + \rho_b}{2} \tag{3-45}$$

In this work, the values of $\alpha = 1$ and $\beta = 2$ are used. Previous works on SPH modeling of solids have indicated that the optimum value for *n* (from 3-36) is between 1.0 and 4.0 [39][40]. In this work, *n*=2.5 provides an un-oscillated solution.

As an example to display the effect of the artificial stress method in resolving the numerical oscillations, a 3m in 5m two-dimensional block modeled using 6161 SPH particles is under tensile load of $\sigma_0 = 1\ KPa$. The modulus of elasticity is set at $E = 10\ MPa$. Results are shown in Figure 3-12.

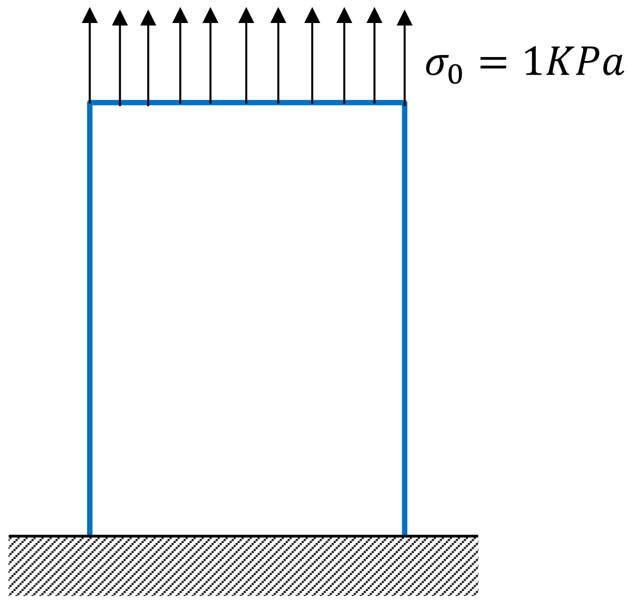

Figure 3-11: Schematic representation of the example test: a 3m in 5m 2D block under tensile stress

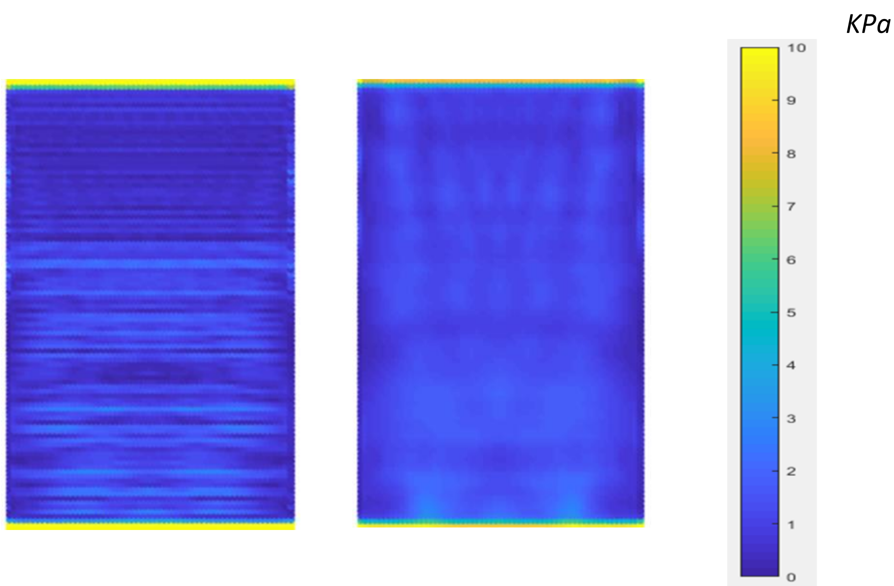

(a) (b)

Figure 3-12: Uniaxial stress contour (a): before and (b): after adding the artificial stress term. The numerical oscillations that are present in (a) have been damped out in (b).

3.4.2.4 Uniform response

In a simple uniaxial loading test depicted in Figure 3-11, the stress waves were initiated at the top and gradually propagated downwards. This causes a spatial variation in the stress value throughout the testing specimen in the early stages of response (Figure 3-13).

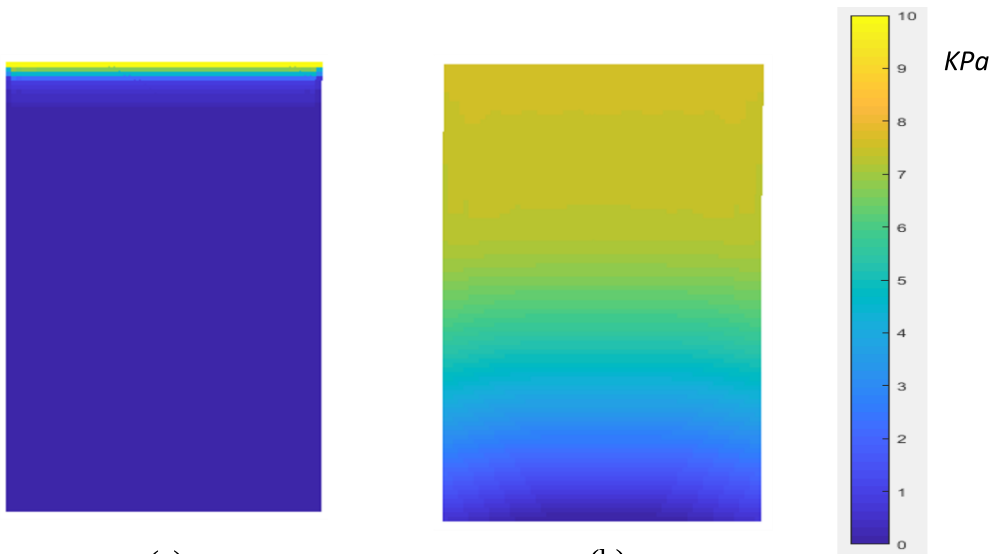

(a) (b)

Figure 3-13: (a): von Mises stress contour at (a): *t*=0, which represents the initial response. As time goes on (in (b)) the stress wave propagates through the solid medium.

Uniform state response is reached eventually when the solid body represents a spatially uniform stress field (Figure 3-14(b)). From this point on, as the uniaxial loading increases, the magnitude of stress will increase uniformly throughout the solid body. All the desired parameters should be computed after the uniform state is reached.

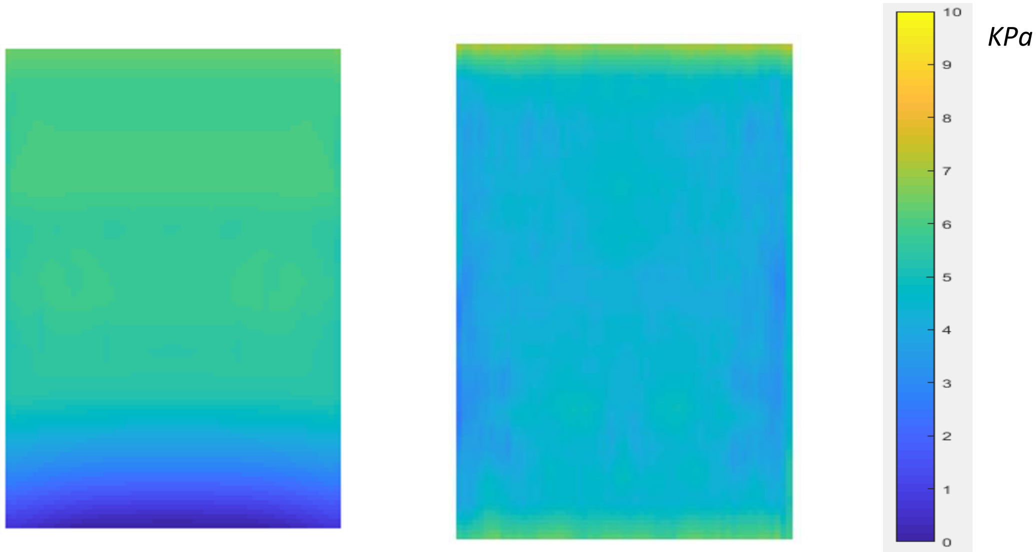

(a) (b)

Figure 3-14: The von Mises stress contour (a): before reaching the uniform state, and (b): after reaching the uniform state. All the desired parameters should be calculated after the uniform state is reached.

3.4.2.5 Fracture mechanics applied to SPH

Introducing cracks into SPH method

In this work, the visibility criterion was employed to introduce a strong discontinuity (crack) into the SPH model. Based on this criterion, the domain of influence of node I is defined as the nodes that are "visible" from node I. As depicted in Figure 3-15, the crack makes the dashed area "opaque", indicating that the nodes located in that area are not considered in the domain of influence of the node I.

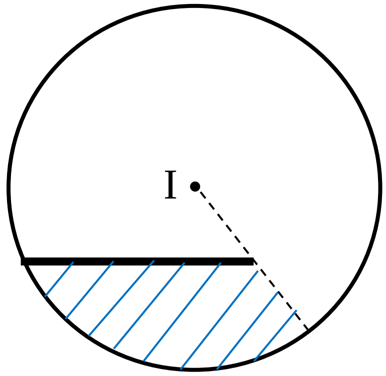

Figure 3-15: The domain of influence of node I in the presence of a crack; the dashed area is "invisible" from node I and thus out of its domain of influence

SIF calculation using SPH

Discretized form of the potential energy per thickness can be written as:

$$\widetilde{U} = \frac{1}{2}\sum_{j}^{N} \sigma_{\alpha\beta}^{j}\, \epsilon_{\alpha\beta}^{j}\, \frac{m_j}{\rho_j} \tag{3-46}$$

After calculating the potential energy, $\frac{\partial U}{\partial a}$ can be approximated as:

$$\frac{\partial U}{\partial a}(a) \approx \frac{-\frac{3}{2}U(a)+2U(a+\Delta x)-\frac{1}{2}U(a+2\Delta x)}{\Delta x} \tag{3-47}$$

Using (3-47), the stress intensity factor will be determined.

3.4.3 Comparison between XFEM and SPH

Various studies have been done to compare the effectiveness of SPH and FE family of methods in solving different engineering applications [41]; however, limited attention has been dedicated to meticulously highlight the potentials and drawbacks of SPH versus XFEM in the fracture mechanics application. Although previous modeling works have roughly pointed out the differences between these two numerical methods [42], a comprehensive comparison is still missing.

In order to quantitatively compare the numerical efficiency of SPH and XFEM in solving a linear elastic fracture problem, and to explore the computational possibilities that are available for food breakdown application, two benchmark tests were designed. These tests were solved using our SPH and XFEM code implemented in MATLAB. The relevant parameters were identified and compared against the analytical solution, and finally, the sensitivity of the solution to the geometrical variables were investigated.

3.4.3.1 Benchmark tests

Pure mode I

As depicted in Figure 3-16, a 10mm in 10mm square, fixed at the bottom, with an initial edged-crack of size a, located horizontally, is subjected to the tensile stress of σ_0. A two-dimensional plane-strain formulation is assigned to this solid block. The modulus of elasticity is set at $E = 10\ MPa$ and the Poisson's ratio at $\nu = 0.3$. The crack propagation in this case is a pure mode I fracture (Figure 3-16).

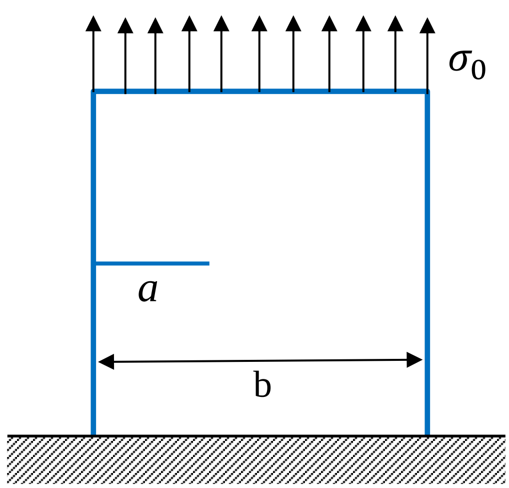

Figure 3-16: Pure mode-I benchmark test

The analytical solution for K_I can be written as [43]:

$$K_I = \left[1.12 - 0.23\left(\frac{a}{b}\right) + 10.56\left(\frac{a}{b}\right)^2 - 21.74\left(\frac{a}{b}\right)^3 + 30.42\left(\frac{a}{b}\right)^4\right]\sigma_0\sqrt{\pi a} \qquad (3\text{-}48)$$

The following values are used here: a=1, b=10, and $\sigma_0 = 1\ KPa$, resulting in the analytical value of $K_I = 0.6634$. The problem (Figure 3-16) is solved using XFEM and SPH and the results are compared against the analytical solution.

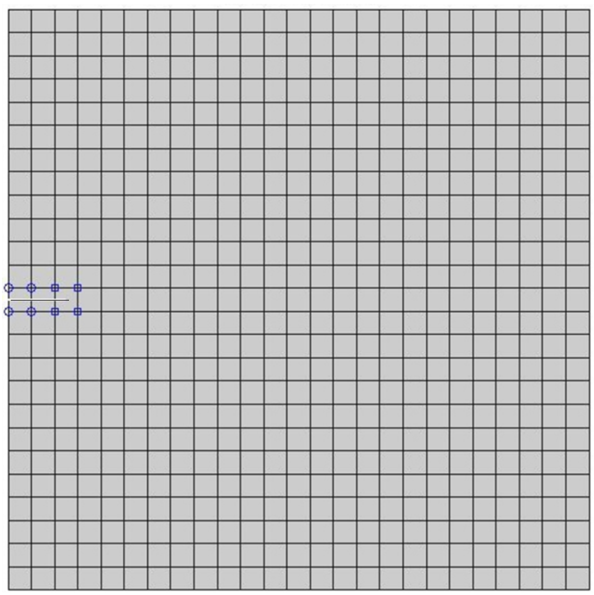

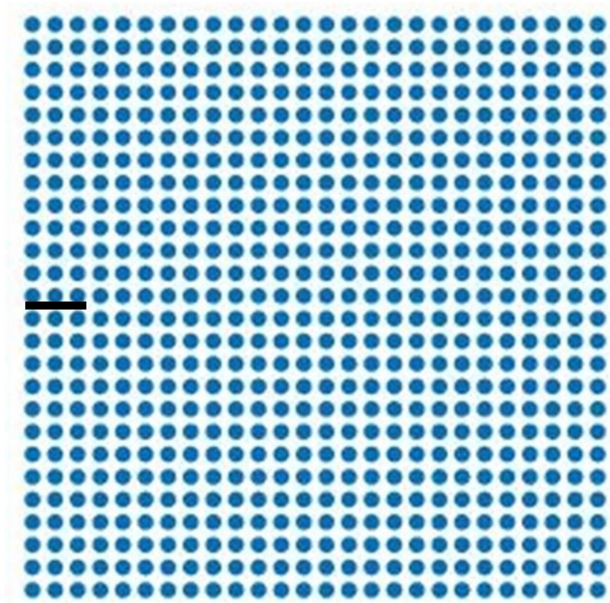

Figure 3-17: Initial configuration of XFEM mesh and SPH particles. a) A 25 in 25 elements XFEM mesh, b) a 26 in 26 particles SPH domain

Figure 3-18 represents the amount of KI divided by its expected analytical value (normalized KI), calculated using SPH and XFEM method. The result from XFEM converges to 1.023, implying a 2.3% deviation from the analytical solution. The SPH solution converges to 0.953, implying -4.7%

error. The previous modeling works have measured the error as 20-30% [44]. This indicates that our modification approach was able to improve the solution for KI by around 15%.

The main source of error in SPH solution comes from the artificial viscosity and artificial stress terms added to the momentum equation (3-36). Despite the fact that adding these terms causes error in SPH solution for stress intensity factor, it plays an essential role in improving the numerical oscillations and instabilities. Therefore, the use of artificial viscosity and artificial stress, and the errors associated with them are inevitable.

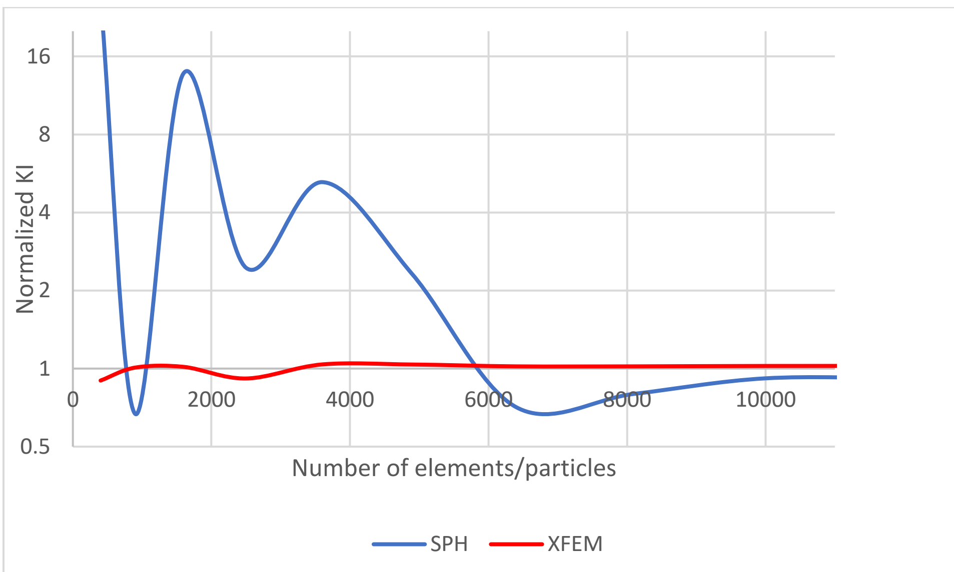

Figure 3-18: The normalized value of KI solved using SPH (in blue) and XFEM (in red)

As it can be observed from Figure 3-18, the XFEM solution requires a lower mesh resolution (3600) to converge, compared to the SPH solution (8100).

The sensitivity of the solution to the geometrical factors (the ratio of the height to the width of the testing subject in this case) is tested and the result is presented in Figure 3-19.

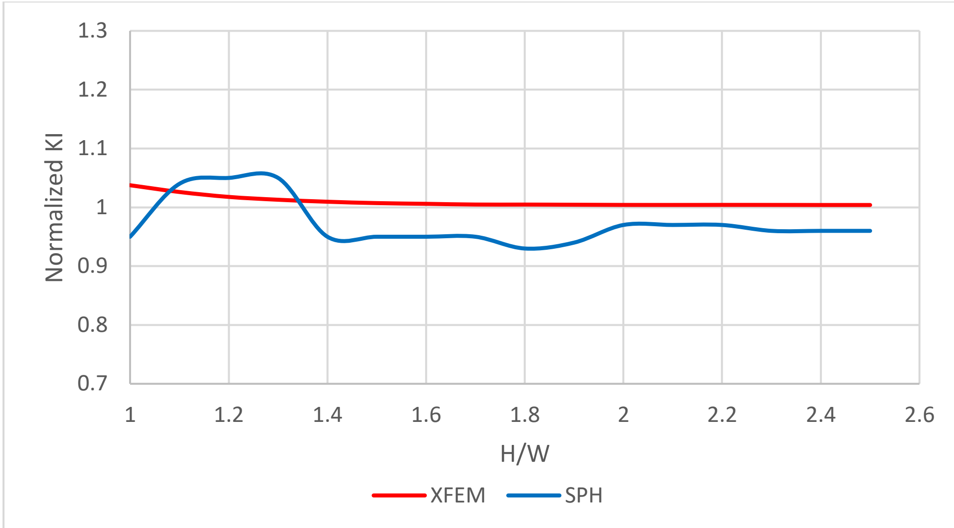

Figure 3-19: Normalized KI value for different height to width ratios for XFEM (in blue) and SPH (in red)

Figure 3-20 shows the graph of von-Mises stress field calculated using a) XFEM and b) SPH method. As we can see, the XFEM provides a more accurate solution for the stress field around the crack tip, which rises from the fact that the crack tip formulation in the XFEM is enriched based on “a priori” analytical solution. The crack applied to SPH is able to represent the discontinuity in stress calculation, however, the stress field solution around the crack tip does not simulate the exact analytical solution. Apart from that, both methods provide accurate solution for the stress field of the points far from the crack tip. A more detailed comparison of the stress solution is presented in Figure 3-28.

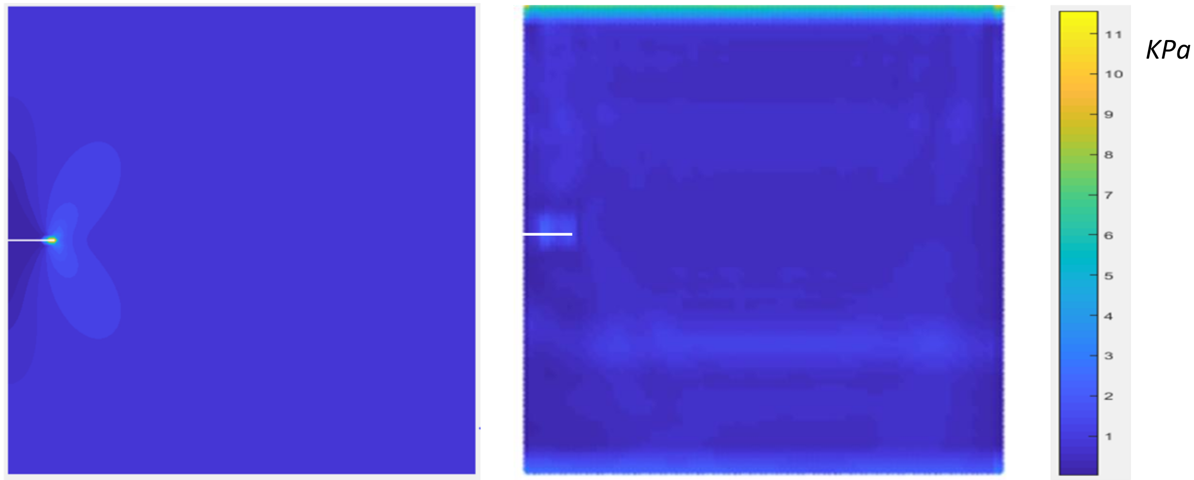

Figure 3-20: von Mises stress from a)XFEM b)SPH model

Another major factor that is worth investigating is the computational cost associated with each method. Generally speaking, the particle-based methods are known to have a higher computational cost and SPH is no exception. The benchmark problem discussed here takes 4.16 s for XFEM model and 2505.3 s for SPH model (Figure 3-21).

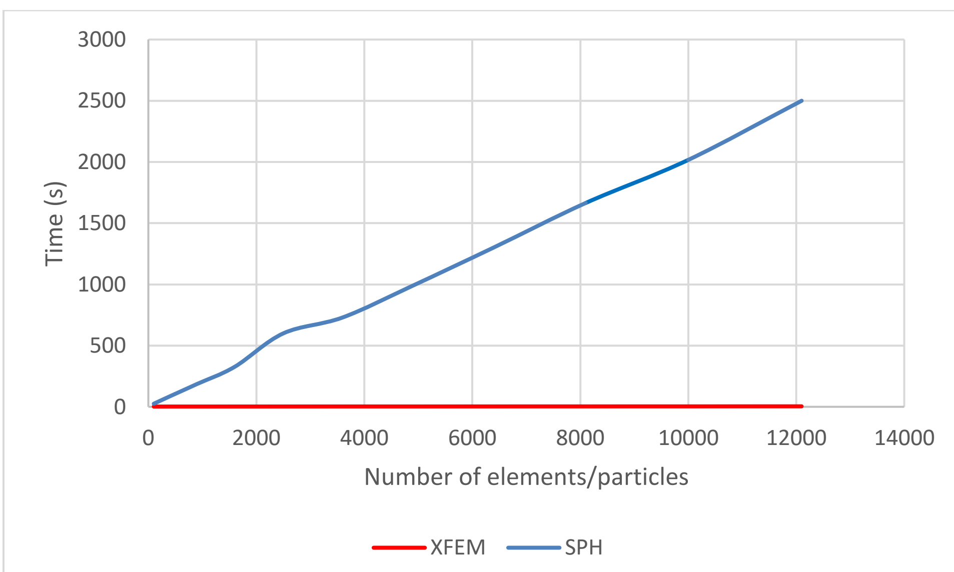

Figure 3-21: Computational cost of using SPH and XFEM

Mixed mode

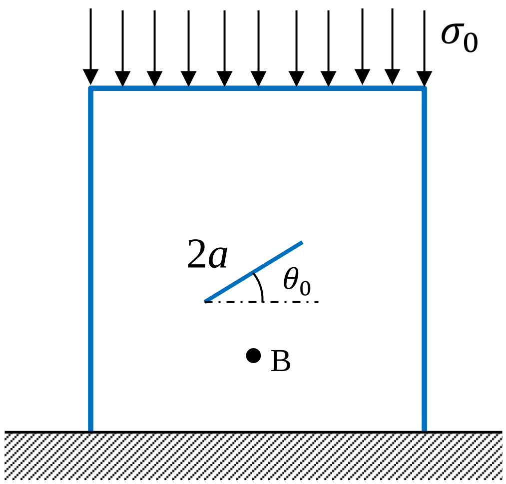

Figure 3-22: Mixed-mode benchmark test

The analytical solution for K_I and K_{II} in the presented mixed-mode problem can be written as [43]:

$$K_I = \sigma_0 cos^2\theta_0\sqrt{\pi a} \tag{3-49}$$

$$K_{II} = \sigma_0 sin\theta_0 cos\theta_0\sqrt{\pi a} \tag{3-50}$$

Solving (3-49) and (3-50) for a=0.1 and $\theta = {}^{\pi}/_{4}$, we get $K_I = 0.626498$, and $K_{II} = 0.626498$ as the analytical solution.

Figure 3-23 represents the normalized K_I, calculated using SPH and XFEM method. The result from XFEM converges to 0.964, implying a -3.6% deviation from the analytical solution. The SPH solution converges to 0.934, implying -6.6% error.

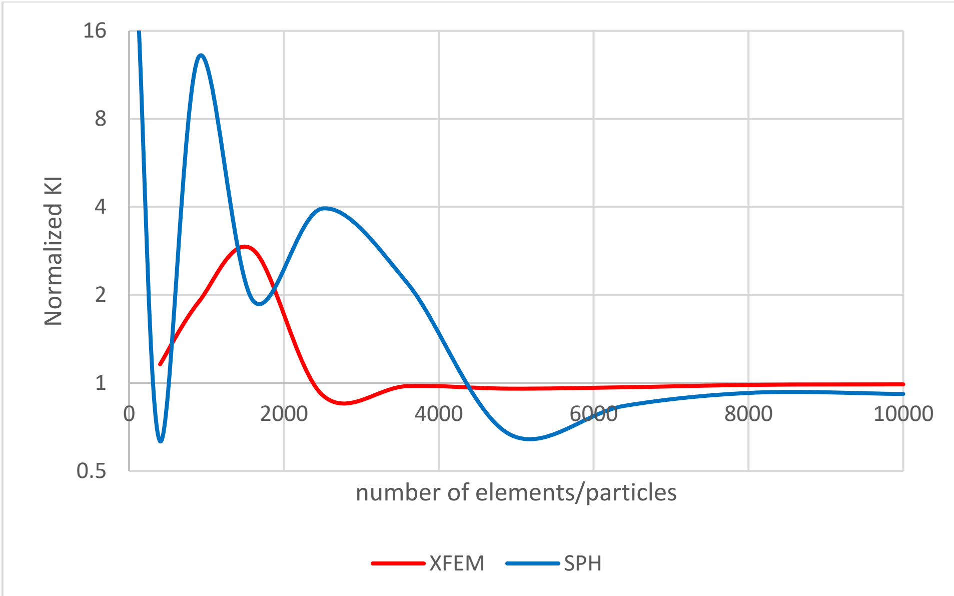

Figure 3-23: The normalized value of KI solved using SPH (in blue) and XFEM (in red)

The calculated normalized K_{II} is shown in Figure 3-24. The result from XFEM converges to 1.028, implying a 2.8% deviation from the analytical solution. The SPH solution converges to 0.947, implying -5.3% error.

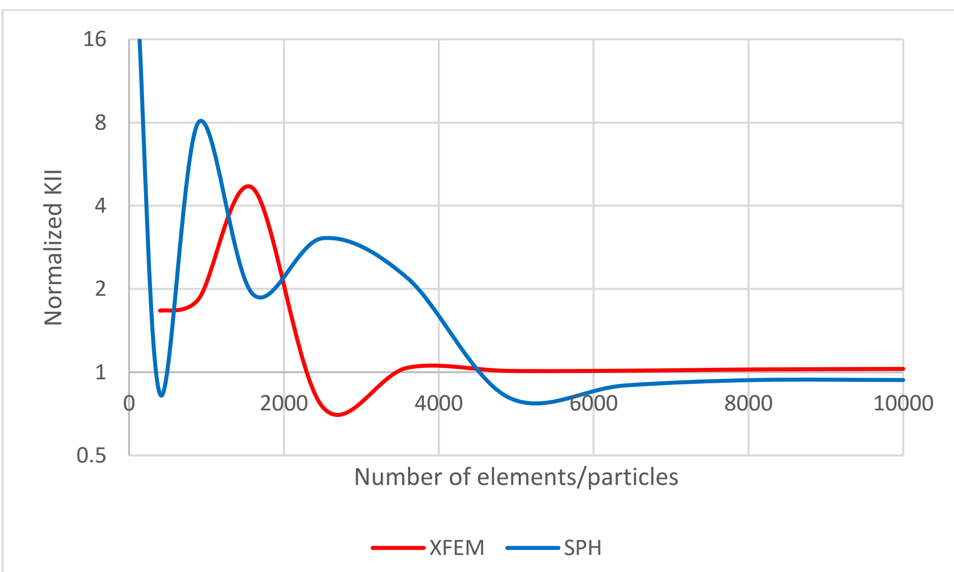

Figure 3-24: The normalized value of KII solved using SPH (in blue) and XFEM (in red)

The sensitivity of the solution to the inclination angle is tested and the result is presented in Figure 3-25 and Figure 3-26.

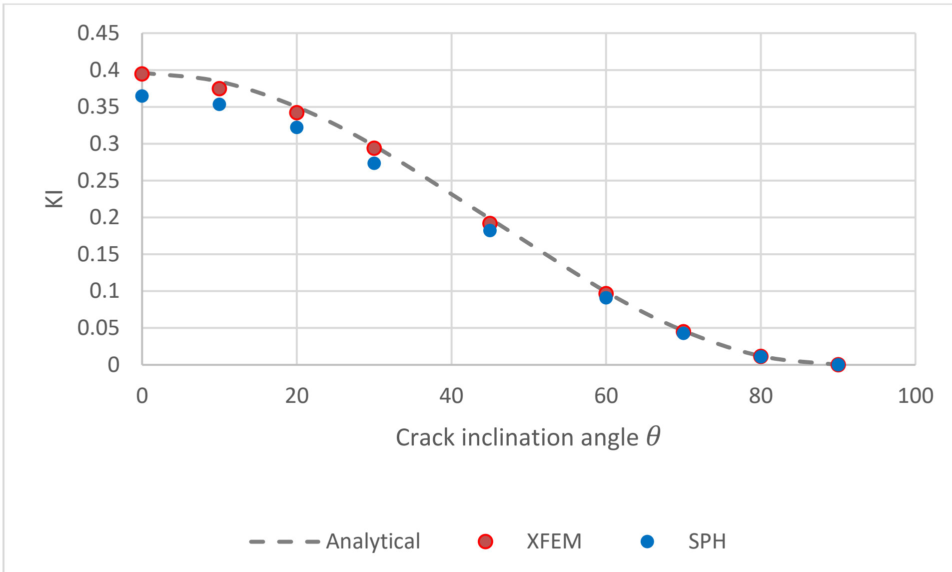

Figure 3-25: KI calculated for different inclination angles using XFEM (red) and SPH (blue)

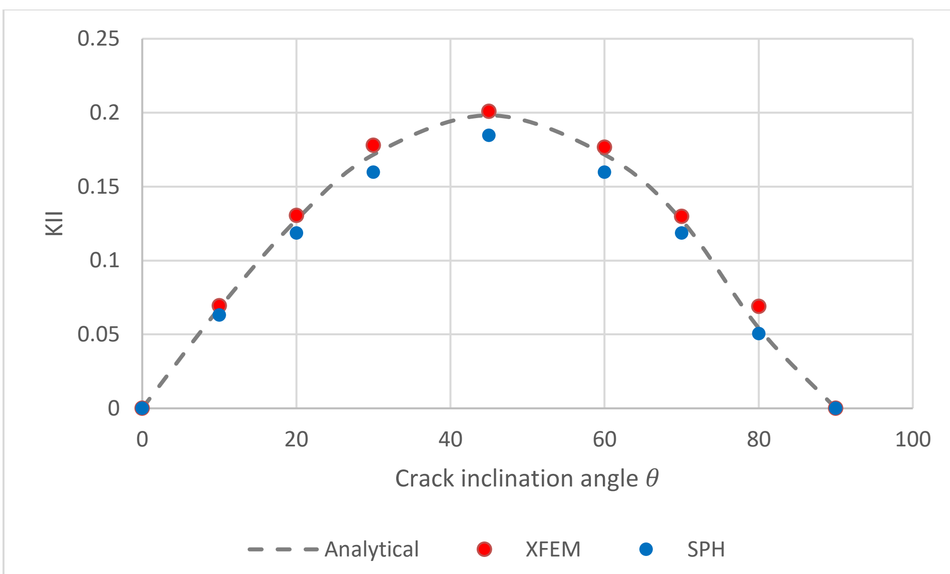

Figure 3-26: KII calculated for different inclination angles using XFEM (red) and SPH (blue)

Figure 3-27 presents the von Mises stress field calculated using XFEM and SPH model. Similar to the stress calculation for the previous test, XFEM model provides a more accurate calculation for the stress field around the crack tip. Further information is provided in Figure 3-28.

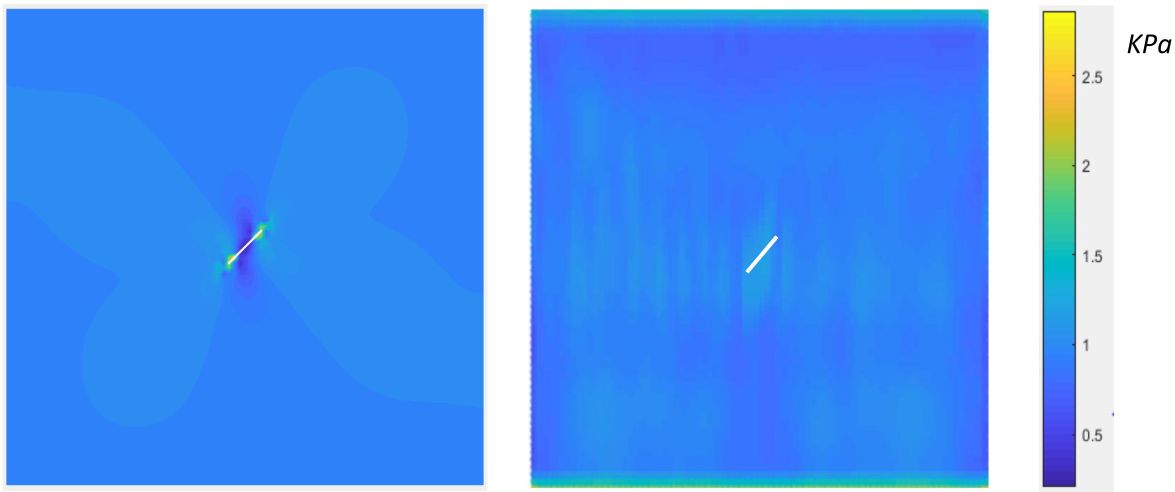

Figure 3-27: von Mises stress contour a) XFEM, b) SPH

The accuracy of each method in calculating the stress intensity factor shows their effectiveness in simulation of the crack propagation. However, a more important factor that directly affects the measurement of occlusal force is the precision of calculating the axial stress across the solid body. Therefore, the accuracy of axial stress calculated using XFEM and SPH will be compared in the next step.

The analytical solution for the principle axial stress, for a point distant from the boundaries (point B on Figure 3-22), can be written as (3-51):

$$\sigma_{y,exact} = E\frac{vt}{L} \tag{3-51}$$

where E is the modulus of elasticity, L is the specimen height, v is the velocity applied to the top boundary, and t represents the loading duration. Figure 3-28 compares the axial stress, calculated using SPH and XFEM, against the analytical prediction from (3-51).

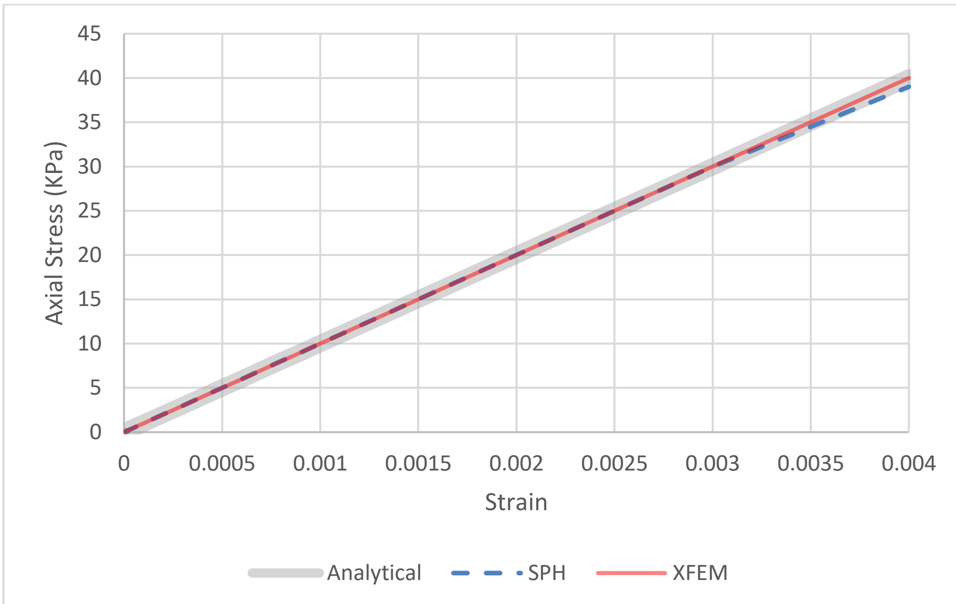

Figure 3-28: The axial stress calculated using the analytical, XFEM, and SPH solution

Figure 3-28 shows a linear increase in axial stress with no significant oscillations for both XFEM and SPH solutions. Although, it is worth mentioning that the SPH graph represents some insignificant oscillation at the beginning. The error approaches to -0.9% for XFEM and to -1.3% for SPH.

From the measurements of the stress intensity factor, which shows how successfully the numerical method can maintain the correlation between the masticatory performance and the occlusal force calculation, we can see that the XFEM provides a slightly more accurate solution. The stress-strain curve on the other hand, does not represent any significant advantage for any of the numerical methods. This suggests that the source of error in the SPH solution for the stress intensity factor most probably comes from the way we modelled the discontinuity in the SPH model (3.4.2.5).

Both of the numerical methods that we studied are capable of measuring the masticatory performance and the occlusal force, which is the main goal of this thesis. Meanwhile, it is noteworthy that the model we are building here is eventually intended to be coupled with the SPH swallowing model [45], to represent a detailed simulation of oral food processing. Keeping this in mind, SPH method seems to be a more promising approach to model food breakdown, as it is known to be more powerful in solving multi-physics problems and problems containing moving boundaries. In addition, SPH formulation enables us to track the history of the particles over time. In spite of the flexibility that SPH method provides, the stability and accuracy analysis is required before its application to the problem.

3.5 Modeling fracture using SPH

So far, we investigated the solution for a single-crack fracture problem. In reality, solid bodies, and food materials in particular, contain incipient flaws. The application of fracture to the SPH method starts by assigning incipient flaws to our brittle solid model. In this work, we assume that a probability distribution function [8] (4-4) defines the most likely number of flaws per unit volume that are having failure strains lower than ϵ.

$$n(\epsilon) = k\epsilon^{m} \tag{3-52}$$

where *m* and *k* are experimental material properties. This Weibull function is isotropic, indicating that it has no information about the location and orientation of any given flaw.

When the local tensile stress reaches the activation point, a crack is allowed to propagate at a constant velocity C_g, usually set at 0.4 times the speed of longitudinal elastic wave.

In this work, a modified format of Grady-Kipp [8] damage evolution model is employed to represent the fracture propagation in SPH model. Based on this model, *D(t)*, the scalar damage parameter that describes the volume-averaged micro-fracture of the material represented by each SPH particle, can be written as:

$$\frac{dD^{1/3}}{dt} = \frac{m+3}{3}\alpha^{1/3}\epsilon^{m/3} \tag{3-53}$$

where ε is the tensile strain and α, a material fracture constant can be written as:

$$\alpha = \frac{8\pi C_g^3 k}{(m+1)(m+2)(m+3)} \tag{3-54}$$

where C_g is the constant crack growth speed, and *k* and *m* are material fracture parameters. To avoid the difficulties associated with the original method, the effective tensile strain is defined as [46]:

$$\epsilon = \sigma_{max}/(K + {}^{4}/_{3}\, G) \tag{3-55}$$

where σ_{max} is the maximum positive component of the stress tensor, and *K* and G are the bulk and the shear modulus of the material. Failure happens when the effective strain surpasses the critical strain threshold.

The damage parameter ranges between *D*=0 (undamaged structure) and *D*=1 (fully damaged). A common approach to apply the damage evolution to the SPH method is to scale down the stress tensor by (1-*D*). This approach will equally affect all the stress components (tensile, compressive, and shear terms). However, a fractured structure is still capable of transferring the compressive load in the damaged region. Therefore, in this work, only the tensile component of stress tensor will be modified by the damage factor:

$$\sigma_D = (1 - D)\sigma \tag{3-56}$$

(3-56) indicates that particles with D=1 act as fluidic particles and do not feel the tensile or shear stress.

3.6 Validation of our SPH fracture implementation

Before proceeding to the food breakdown simulation, our implementation of SPH fracture model has to be validated against the experimental data. To do so, the fracture formulation is applied to a 200 *mm* in 150 *mm* solid block, modeled using 30,351 SPH particles. Eventually, since the experimental data for the fracture of food materials are not widely available, results from this simulation are compared against the experimental studies on rock-like materials. It is generally known that the sensitivity of the accuracy to the material properties is insignificant, or to be more specific, it is usually overshadowed by the sensitivity to the geometrical properties. To confirm this, the simulation will be done for two different material types, one homogenous and one heterogeneous, in order to check the sensitivity of the model to heterogeneity.

As a homogeneous material, we are going to apply the material properties of Basalt, a dark fine-grained rock, to our SPH model and simulate its failure process and eventually, compare the simulated results against the experimental studies.

Table 3-1 represents the mechanical properties of Basalt that are applied to our SPH model [47].

Density ($\frac{g}{cm^3}$)	Modulus of elasticity (GPa)	Uniaxial compressive strength (MPa)	Poisson's ratio
2.7	95.2	352.6	0.20

Table 3-1: Mechanical properties of Basalt under uniaxial compression

The axial stress-strain curve from the simulated results and the experimental study (from [47]) on Basalt is presented in Figure 3-29.

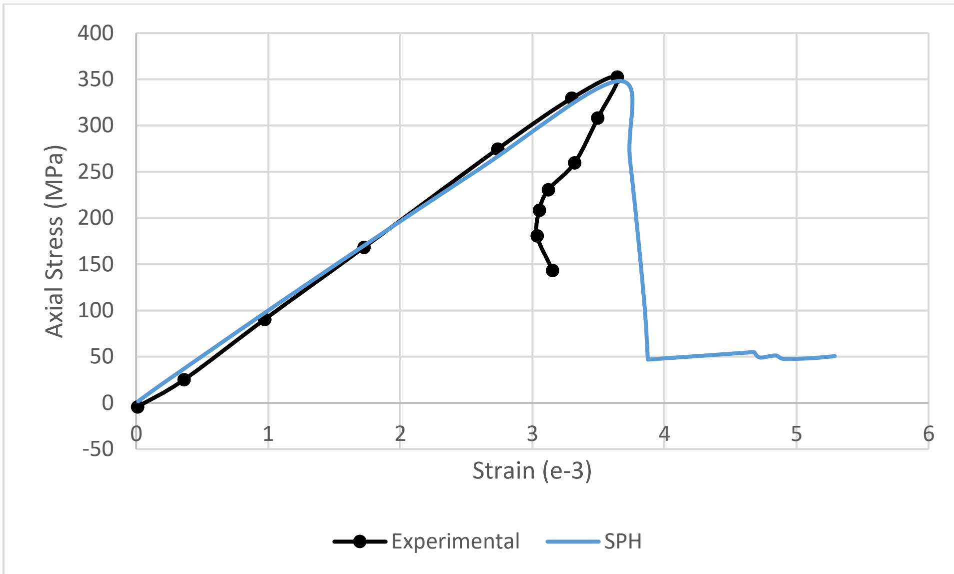

Figure 3-29: Axial stress versus strain (Basalt)

As a heterogeneous material, the failure process of Tennessee Marble was simulated using our SPH implementation. Figure 3-30 represents the axial stress-strain curve from the simulated and the experimental data (from [47]).

Table 3-2 shows the mechanical properties of Tennessee Marble.

Density $(\frac{g}{cm^3})$	Modulus of elasticity (GPa)	Uniaxial compressive strength (MPa)	Poisson's ratio
2.7	51.5	110.91	0.27

Table 3-2: Mechanical properties of Tennessee Marble

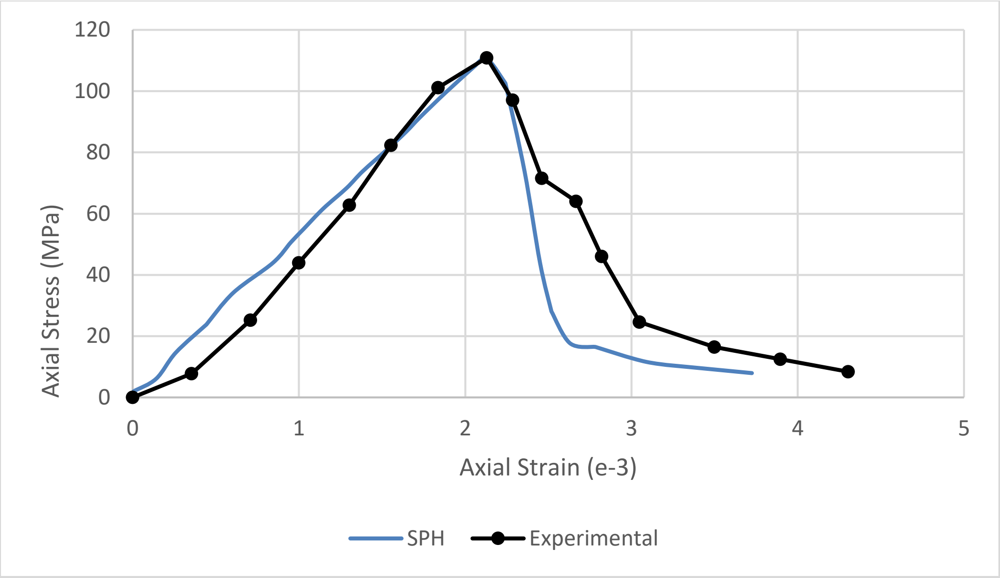

Figure 3-30: Axial stress versus strain curve (Tennessee Marble)

Besides Basalt and Marble, the simulation was also done for Charcoal and Limestone (relevant mechanical properties can be found in [47]). Figure 3-31 represents the simulated axial stress-strain curve for a variety of material properties. The simulated results show -1.4%, -1.4%, -1.5%, and -1.2% error in calculating the maximum axial stress for Basalt, Limestone, Charcoal, and Marble respectively.

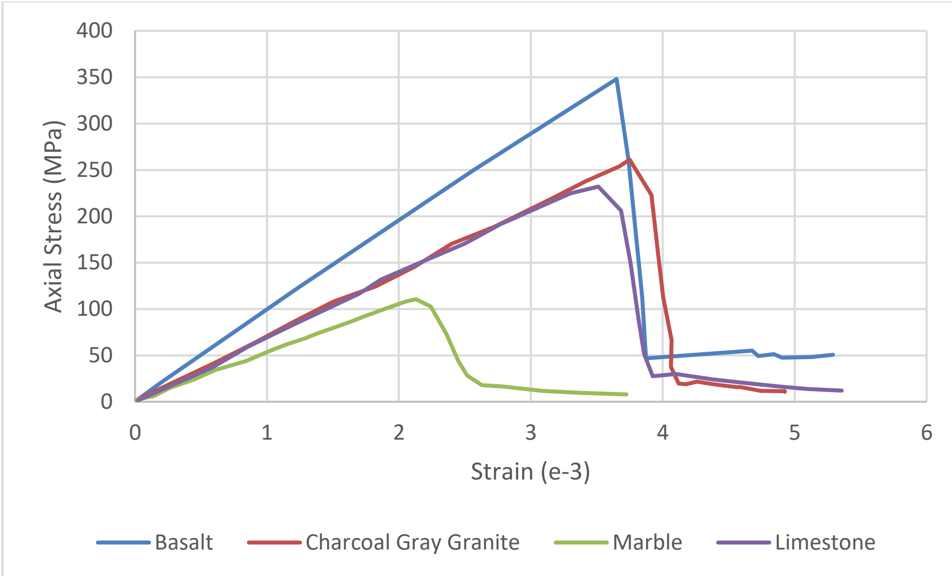

Figure 3-31: Simulated axial stress-strain curves for different materials

The predicted fracture evolution of Basalt specimen (homogenous) is presented in Figure 3-32.

Figure 3-32: The evolution of simulated fracture process for Basalt

As expected, failure happened in the oblique plane, perpendicular to the direction of the maximum principal stress. The simulated fracture is in accordance with the previous experimental studies on the behavior of brittle materials under compressive loading (from [48]).

Besides the modulus of elasticity, the sensitivity of the results to the variations in other material properties, such as the Poisson's ratio, has been discussed in the previous works. It has been shown that for incompressible rubber-like solids (with Poisson's ratio around 0.5), a slight change in the Poisson's ratio can change the modeling results considerably [49]. However, previous parametric studies on the brittle materials (0.1< Poisson's ratio<0.3) have shown that the final modeling results are not sensitive to the variations in the bulk modulus and the Poisson's ratio [50].

Overall, we can conclude that the accuracy of our SPH implementation in simulating the fracture process in brittle materials is not sensitive to the variation in the material properties. Therefore, it is safe to use it for food breakdown modeling.

Chapter 4: Numerical Simulation of Food Breakdown and the Method to Measure the Occlusal Force and the Masticatory Performance

4.1 SPH and FEM contact algorithm

In order to measure the occlusal force, and as the first step toward integrating the food breakdown model into the biomechanical model of the masticatory system, the SPH model has to be coupled with a FE mesh. An effective coupling between these two models requires a valid contact detection algorithm as well as an accurate force calculation schema.

4.1.1 Contact detection

In order to preserve the exchanged force, a node-to-node contact algorithm is utilized in this work [51]. Based on this algorithm, the two objects come into contact with each other when the FE nodes enter the particles' support domain (1.5 times the element spacing in this case)(Figure 4-1). Any node that is close enough to the accounted particle will be added to its neighboring particles list.

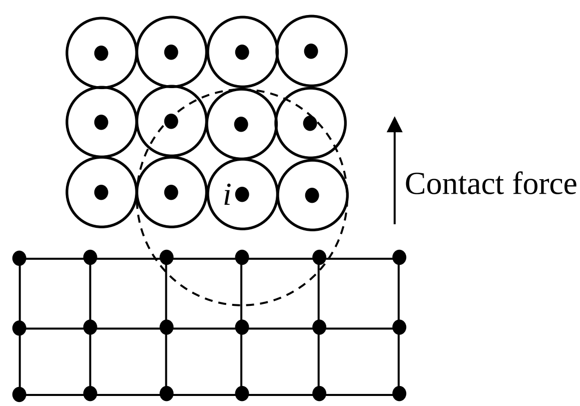

Figure 4-1: SPH to FEM contact

4.1.2 Contact force

The first step in calculating the contact force is the determination of contact potential ϕ:

$$\phi(x_i) = \sum_j^{NCONT} \frac{m_j}{\rho_j} K \left(\frac{W(r_{ij})}{W(\Delta p_{avg})}\right)^n \tag{4-1}$$

where *NCONT* contains the neighbor particles to the particle *i*, belonging to a different body. Δp_{avg} represents the average value of the smoothing length, and K is the contact stiffness penalty. The body force is calculated as the gradient of the potential:

$$b(x_i) = \nabla\phi(x_i) = \sum_j^{NCONT} \frac{m_j}{\rho_j} K \frac{W(r_{ij})^{n-1}}{W(\Delta p_{avg})^n} \nabla_{x_i} W(r_{ij}) \tag{4-2}$$

The contact force is written as (4-3):

$$Q(x_i) = \sum_j^{NCONT} \frac{m_j}{\rho_j} \frac{m_i}{\rho_i} Kn \frac{W(r_{ij})^{n-1}}{W(\Delta p_{avg})^n} \nabla_{x_i} W(r_{ij}) \tag{4-3}$$

The contact forces will later be added to the SPH's momentum (3-23), and to the FE's external force matrix.

4.1.3 Fragment size measurement

After the solid body is fully fractured, in order to assess the masticatory performance, we need to identify the particles that are forming unified fragments. A fragment is defined as a volume of particles, still connected by strength and bounded by a strength-less region.

The fragment search algorithm used in this work is based on a friends-of-friends algorithm which searches for the contiguous fragments. Based on this algorithm, we start from an undamaged particle ($D < 1$) and search for its undamaged neighbors. This will be followed by finding the undamaged neighbors of the undamaged neighbors. This procedure goes on until there is no undamaged neighbor left.

The search algorithm described above does not require the fragments to be distinguishably separated in space in order to be detected.

4.2 Food breakdown using SPH

4.2.1 Modeling specification

The food morsels are considered as 10mm in 10mm solid blocks (to imitate the clinical experiments from [52]), and are modeled using 10,201 SPH particles. In order to keep the loading in the quasi-static range, the loading rate was set at $0.01s^{-1}$, and the axial velocity at the top boundary was set at 0.1 $\frac{m}{s}$. The simulation runs for a maximum duration of 0.4 s, which is the maximum duration of a single chewing stroke. The simulation stops at any point before 0.4s when the solid body reaches the complete failure state.

The common foods that are clinically used for measuring the masticatory performance include almonds, carrots, variety of cheese, and peanuts. A number of artificial food materials have also been used to provide information on the masticatory performance [53].

Table 4-1 represents the physical and mechanical properties of almond [54], raw carrot [55], and roasted peanut [56].

Food	Modulus of Elasticity (MPa)	Toughness ($\frac{J}{m^3}$)	Density ($\frac{g}{cm^3}$)
Almond	21.57	245.8	1.015
Raw carrot	4.57	440.0	1.04
Roasted peanut	23.90	214.3	1.088

Table 4-1: Mechanical and physical properties of brittle food materials

Note that the values reported as the mechanical properties of food materials are not universally applicable. In fact, due to the variation in the moisture content and the level of porosity, these values may vary intensely in different samples.

4.2.2 Masticatory performance and occlusal force measurements

Figure 4-2 schematically represents the calculation process of occlusal force and masticatory performance.

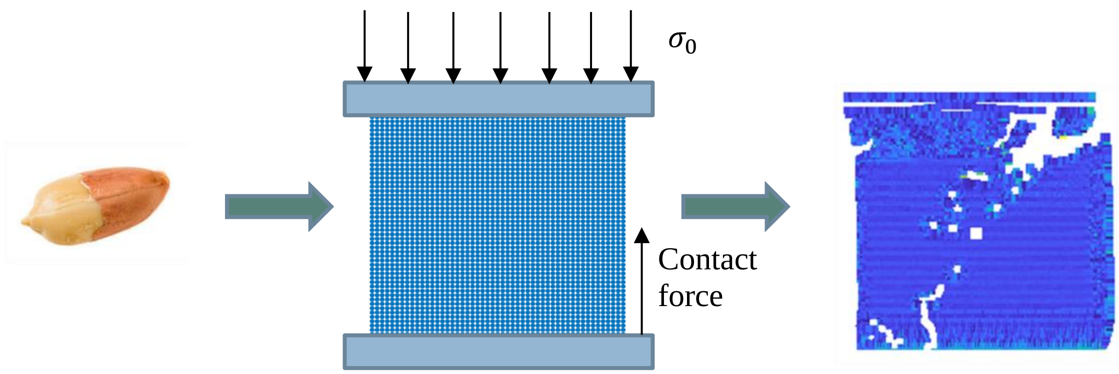

Figure 4-2: Food breakdown model

Based on the procedure described in 4.1.3, the surface area of the resulting fragments were measured. The fragmented shape of peanut morsel is depicted in Figure 4-3. Here, as an indicator of the masticatory performance, we are going to measure the root square of the change in the specific surface of the food morsels (Equation 4-4).

$$Masticatory\ performance = \sqrt{|Specific\ surface_2 - Specific\ surface_1|} \qquad 4\text{-}4$$

Specific surface is defined as the apparent surface area of the fragment divided by its volume. $Specific\ surface_1$ represents the specific surface of the initial food sample, and $Specific\ surface_2$ represents the specific surface of the largest chunk following the food breakdown. The algorithm provided in 4.1.3 is used in order to calculate the eventual surface of the food particles following the chewing stroke.

The simulated results will be validated against the experimental results from [52] where the measurements were done on food samples enveloped in plastic bags in order to discard the softening effects of saliva.

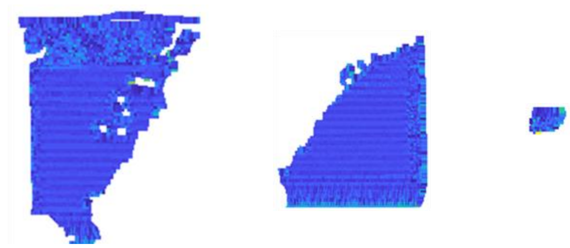

Figure 4-3: Food fragments following one chewing stroke. The size of each fragment will be calculated based on 4.1.3.

Figure 4-4 represents the simulated and the experimental measurements of the masticatory performance versus the modulus of elasticity. The correlation test indicates 84% correlation between the simulated masticatory performance and the modulus of elasticity.

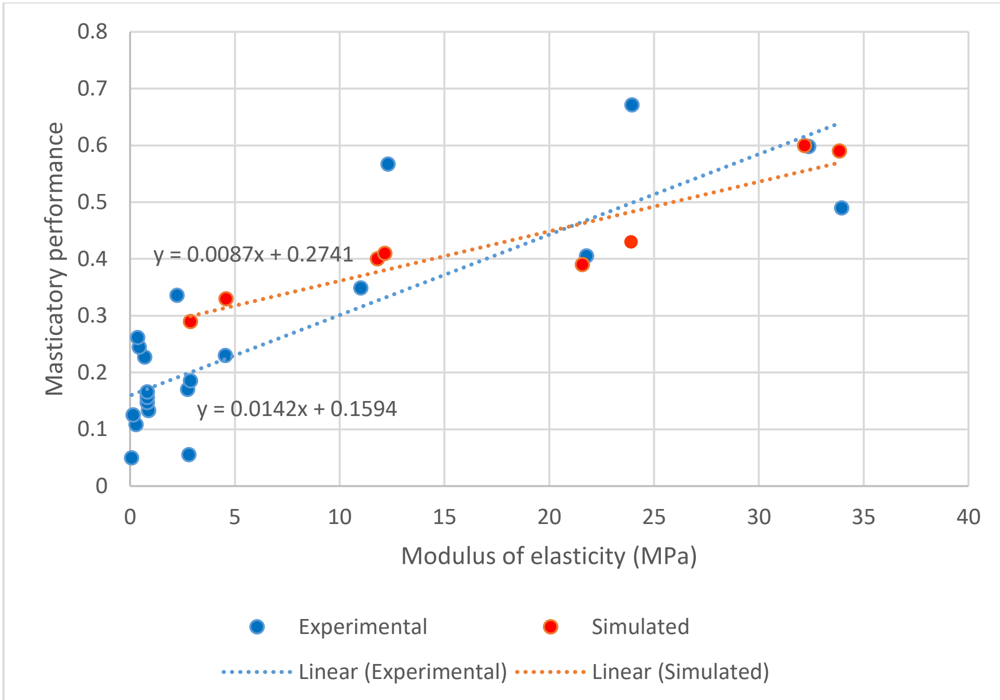

Figure 4-4: Masticatory performance versus the modulus of elasticity for the simulated and the experimental results

The two regression lines fitted to the simulated and the experimental data (Figure 4-4) are significantly different ($p<0.05$). However, the simulation was only done for the food samples that are identified as brittle. Comparing the slope of the simulated results with the experimental data for those brittle materials indicates a higher similarity ($p>0.05$) (Figure 4-5).

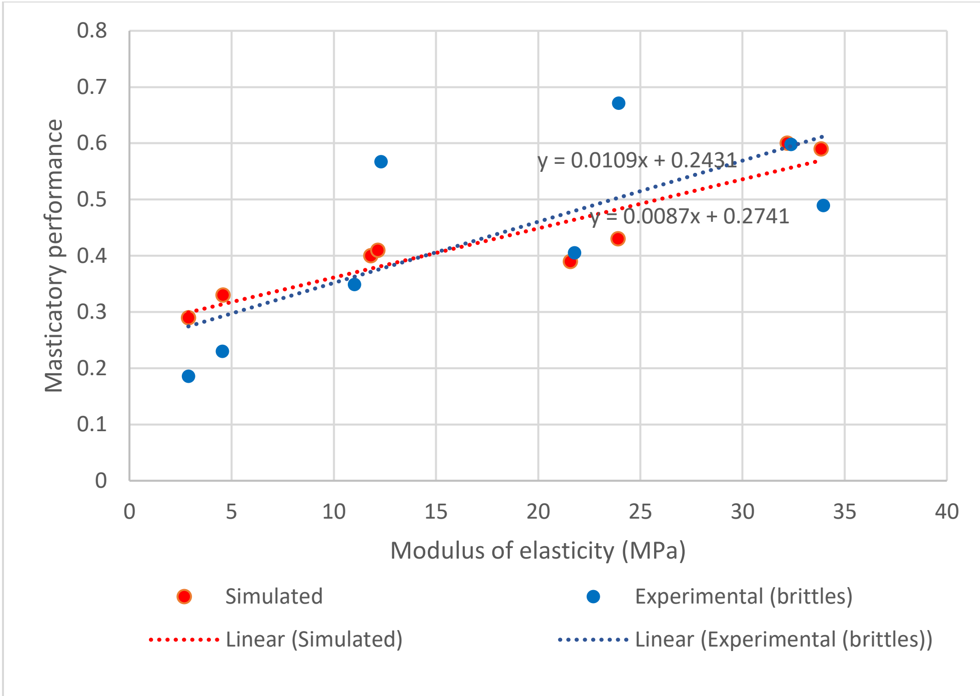

Figure 4-5: Simulated results compared to experimental measurements for brittle food samples

Figure 4-6 represents the simulated occlusal force value for a number of food samples.

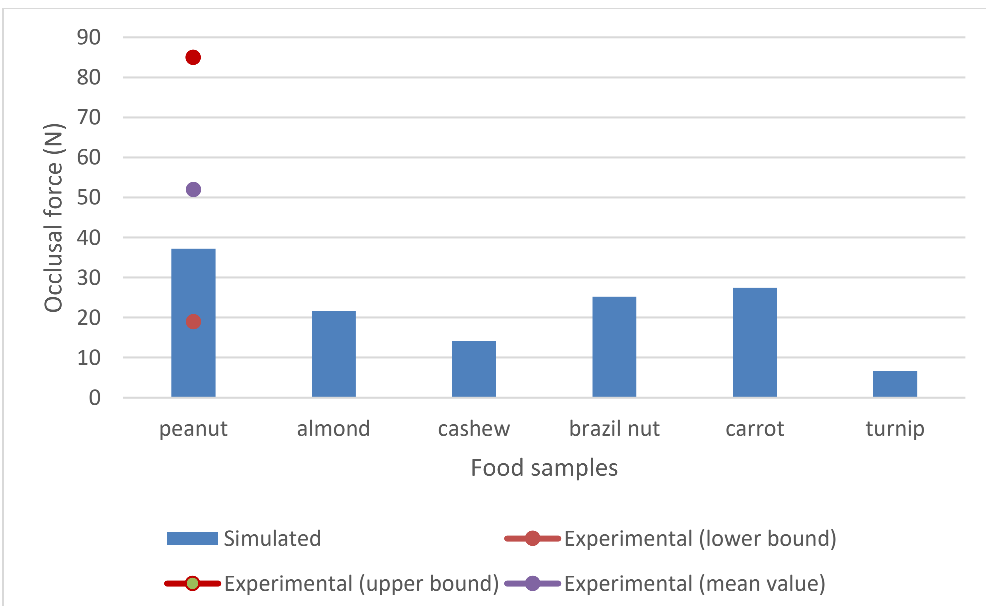

Figure 4-6: Occlusal force measurements

The experimental occlusal force measurements are only available for the peanut and the beef samples (from [57]), as most of the previous studies on the chewing forces have not specified the material of their testing food samples. Since beef in general does not represent brittle behavior, the experimental results for peanut samples are going to be discussed in this work (Figure 4-6).

The comparison between the simulated and the experimental results for peanut from Figure 4-6 shows that the simulated values are smaller than the experimental mean values and that they are between the upper and lower bounds of the reported measurements. However, as the mechanical properties of foods can vary significantly over different samples, we should note that this comparison may not be a reliable approach to validate the simulated results. In addition, the experiments were not necessarily performed using the standard cubic food samples. This can be regarded as another major source of error, as the amount of occlusal force is highly sensitive to the geometrical variations in the food samples. It is also noteworthy that the experimental measurements that are presented in Figure 4-6 were measured using devices embedded in dental prosthetics. Placing the strain gauge transducers inside the subject's natural dentition is ethically prohibited.

Figure 4-7 represents the relationship between the masticatory performance and the occlusal force measured using our SPH model.

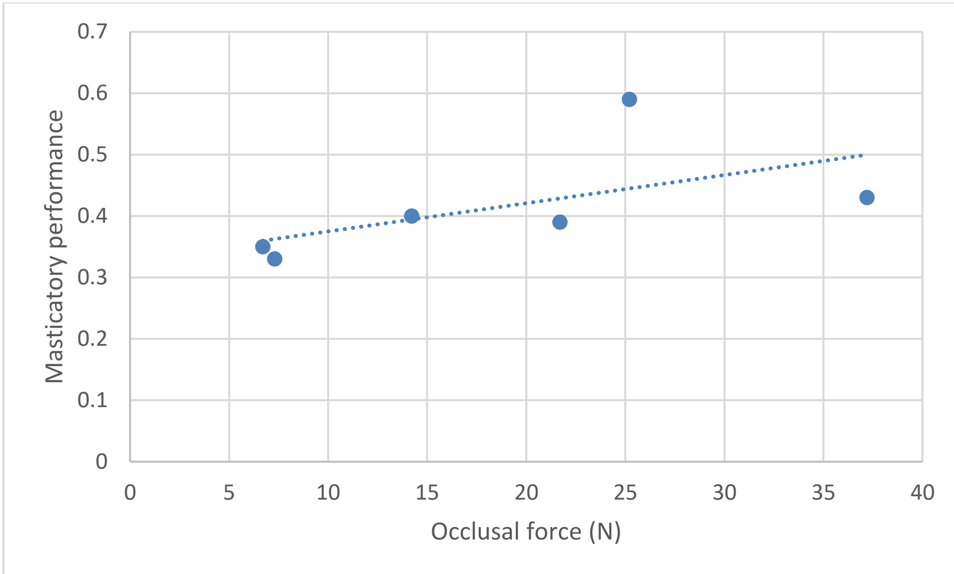

Figure 4-7: Masticatory performance against the occlusal force

From the correlation study, we can see that our simulated masticatory performance and occlusal force are moderately correlated (r=59%). The previous experimental studies have reported a slightly stronger positive correlation between these two factors (r=66%) [4].

The main goal of this thesis was to investigate the possibility of using a two-dimensional fracture mechanics model to evaluate the masticatory ability. Our simulated measurements of the masticatory performance are in accordance with the experimental measurements. However, in order to have a more comprehensive evaluation of the masticatory performance, a model containing all the missing components (saliva and teeth geometry), and proper experimental studies are required.

Considering the current available clinical measurements, the validation of the simulated occlusal force seems to be impracticable. The complexity of the chewing system along with the unethical nature of placing a measurement device inside a healthy subject's mandible, questions the viability of conducting further measurements. Once again, this highlights the importance of assessing the masticatory performance and the occlusal force correlatively. The association between these two objective metrics (Figure 4-7) can be potentially used as an alternative approach to validate the accuracy of our model in measuring the occlusal force.

Chapter 5: Conclusion and Future Work

5.1 Summary

This thesis evaluates the ability of a two-dimensional LEFM model in simulating the oral food comminution. The main goal of this model is to assess the masticatory performance and the occlusal force. It is important to assess these two objective clinical metrics correlatively in order to have a deep understanding of the masticatory ability. The analytical solution for a two-dimensional fracture mechanics problem is not available for all the geometries. This requires the implementation of computational methods to solve our fracture mechanics problem.

A variety of computational methods are available to solve fracture mechanics problems. In order to investigate the computational possibilities, XFEM and SPH method, two methods that employ two distinct approaches, were implemented and their strengths and weaknesses were investigated (Chapter 3). The conventional formulation of SPH for solid deformation suffers from the numerical instability and boundary deficiencies. A number of numerical modifications and studies were performed in order to mitigate the mentioned deficiencies. Two fracture mechanics benchmark tests were solved using XFEM and the modified version of SPH in order to assess the strengths and weaknesses of these two computational methods. Finally, the SPH method was selected to model the food breakdown. The fracture SPH model was validated against the experimental studies on the brittle materials. The sensitivity of the solution to the variation in the material properties was also investigated.

The SPH model was coupled with a FEM model in order to measure the occlusal force (Chapter 4). A fragment detection algorithm was implemented in order to measure the masticatory performance. Finally, the food breakdown was simulated for a number of brittle food materials and the corresponding masticatory performance and occlusal force were measured. The simulated results were compared against the relevant experimental measurements.

5.2 Discussion

5.2.1 Comparison between XFEM and SPH

During the comparison phase, the main focus was on the calculation of the stress intensity factor and the stress analysis. These two factors can be regarded as the determinants of the accuracy of the model in measuring the masticatory performance and the occlusal force, and their correlation. Both numerical methods were capable of calculating the stress intensity factors and the axial stress accurately. Although, it is noteworthy that in order for the SPH model to represent an accurate solution for fracture mechanics problems, a thorough investigation of the relevant parameters and an analysis of the stability and accuracy of its solution for elastic solid deformation, is required.

In this work, the numerical oscillation of SPH solution for elastic solids was improved by adding the artificial stress terms to the momentum equation (3-36). The main drawback of using the artificial viscosity method is the fact that due to its damping effects, it can cause some deviation between the SPH solution and the expected analytical values. Once again, this highlights the importance of performing a thorough numerical study on the relevant artificial stress coefficients (n in 3-36, α and β in 3-44) in order to mitigate the damping effects.

The sensitivity of the accuracy of both methods to geometrical factors is another principal aspect to consider. Figure 3-25 and Figure 3-26 indicate that both solutions are insensitive to geometrical variations as long as the requirement for mesh resolution is met. Overall, it is safe to say that both numerical approaches can be used for the food breakdown application. However, as part of the future work, the food breakdown model is intended to be coupled to the swallowing model in order to develop a comprehensive representation of the human food processing system. This draws attention to the SPH ability to handle moving boundaries and multi-physics problems. Eventually, the SPH method was selected to model the two-dimensional food breakdown.

It is also worth mentioning that the numerical comparison between the XFEM and SPH not only provides valuable insights into their strengths and weaknesses, but also compares the differences between the mesh-based and mesh-free modeling approach, as well as the potential of the extrinsic versus intrinsic enrichment approach.

Figure 3-29 and Figure 3-30 show that our two-dimensional SPH implementation is capable of simulating the fracture propagation for brittle materials. In addition, the solution provided by SPH does not express sensitivity to the variations in the material properties. This is an important factor to consider while studying the mechanical responses of the food samples, since the mechanical properties may vary significantly over different samples.

5.2.2 Food breakdown model

Figure 4-4 represents the masticatory performance measured using the food breakdown simulation as well as the experimental studies. The exact mechanical properties of the food samples are not provided in the experimental literature. Therefore, instead of comparing the simulated and the experimental values of the masticatory performance for each individual food sample, it is more logical to focus on the difference in the trend-line of the masticatory performance versus the modulus of elasticity. From Figure 4-4, the food breakdown simulation represents 84% correlation between the masticatory performance and the modulus of elasticity. The relationship between the masticatory performance and the food material properties has been long debated in the clinical literatures. Although the correlation between them has been clinically observed [52], due to the absence of a reliable means for clinical data collection, the actual relationship is not definitely established. This highlights the potential of the biomechanical modeling approach in studying the complexities of the human masticatory system.

From Figure 4-4, the experimental and the simulated trend-lines are significantly different. The experimental data shown in Figure 4-4 include the measurement for foods with different material characteristics, whereas the food breakdown simulation only targets the brittle materials. Therefore, in order to have a more equitable comparison, we compared our simulated results against the experimental data for the brittle food materials (Figure 4-5). Figure 4-5 shows a higher level of similarity between the experimental and the simulated measurements of the masticatory performance.

Figure 4-6 presents the simulated occlusal force for a number of brittle food materials. The relevant experimental measurements were only available for beef and peanut. Although the simulated results for beef and peanut are within the limits of the experimental measurements, due to the restriction of clinical data, we are not able to validate the simulated occlusal forces at this point. This limitation and the proper approach to overcome it will be discussed in 5.2.3.2 and 5.3.2.

5.2.3 Limitations

The SPH implementation was previously validated against the experimental studies on brittle materials, meaning that the main source of deviation between the food breakdown model and the clinical measurements originates from the 1) modeling simplifications, and 2) imprecision in clinical measurements.

5.2.3.1 Modeling simplifications

The food breakdown model considers the human dentition as a simplified flat surface, whereas the natural human tooth is cusp-shaped. The irregularities in the crown's shape causes stress intensity in both the dentition and the food sample, which can alter the simplified solution. Also, the simplification of the tooth shape to a flat surface hampers the ability of our food breakdown model to measure the tangential component of the occlusal force. The tangential component of the occlusal force is responsible for grinding the food materials. Previous clinical studies on the masticatory forces have measured the tangential force as 8.1 N, the normal force as 59.7 N, and the total masticatory force as 60.2, while chewing carrot [58]. This indicates that although the tangential component is significant, it does not contribute significantly to the overall occlusal force. It is also worth mentioning that the majority of the clinical studies were only capable of measuring the normal component, due to the restrictions in the measuring devices and their placement. The measurement procedure presented in [58] constrains the natural chewing movements of patients. Also, similar to the studies on the normal occlusal force [57], the measurements were done on the dental prosthetics instead of the natural human dentition. This indicates that the current clinical techniques are not able to precisely measure the natural grinding force of the healthy subjects. With these in mind, we can conclude that, any further improvement in the modeling approach presented in this thesis has to be accompanied with a more reliable strategy to measure the relevant clinical metrics.

The simplification of the three-dimensional fracture to the two-dimensional fracture mechanics model may cause inaccuracy in the results. However, it is important to note that moving to a higher dimensional SPH model can increase the computational costs drastically (Figure 3-21). This suggests that building a three-dimensional SPH model requires an efficiency pre-examination.

5.2.3.2 Imprecision in clinical measurements

Besides the modeling simplifications, the other major source of deviation between the simulated and the experimental results comes from the imprecision in the clinical measurements. Both the masticatory performance and the occlusal force measurements are highly sensitive to the initial shape of the food sample. In many cases, shaping a food material into a standard cubical geometry is not feasible. Any irregularity in the sample's initial shape can cause stress intensity, which will eventually lead to inaccurate measurements. The use of artificial foods as the testing sample can facilitate this problem.

Figure 4-6 presents the simulated occlusal force measurement for a number of brittle food samples. The clinical data for the occlusal force measurement on the human dentition is limited and inconsistent across different experimental studies. Although the correlation between the food stiffness and the occlusal force has been clinically observed, the previous experimental studies have not considered the material factor in their experimental designs. In many cases, the material characteristic of the food sample has not been reported, or has been roughly described as "hard" or "soft" material [4]. The relevant clinical measurements were only found for beef and peanut (Figure 4-6). The simulated results are within the limits of the clinical measurements.

Overall, it can be stated that the current available clinical methods to measure the occlusal force are unreliable. Once again, this highlights the potentials of the food breakdown modeling in studying the human masticatory system. In particular, the correlative assessment of the occlusal force and the masticatory performance enabled us to convert the occlusal force to the masticatory performance, which is physically observable and clinically measurable.

5.3 Future work

This section reviews the potential improvements and the possible future applications of this research thesis.

5.3.1 Enhancing the food breakdown model

The current food breakdown model simulates the breakage of the brittle materials following one chewing stroke. A deeper understanding of the masticatory system requires a more comprehensive modeling approach that covers a broader range of food properties and includes all the biomechanical components involved in the human masticatory system.

By adding the viscoelastic material model, the food breakdown model will be able to simulate the breakage of a wider range of materials. However, it should be noted that the masticatory performance experiment might not be the appropriate method to evaluate the efficiency of the masticatory system in processing the non-brittle food materials. Alternative clinical methods, such as measuring color change or sugar loss from a chewing gum, were designed to evaluate the efficiency of the chewing system in processing the viscoelastic food materials.

The chewing process starts with food ingestion and goes on to the point where the food becomes ready to be swallowed. The number of chewing cycles that are required to form a cohesive bolus is another major indicator of the efficiency of the masticatory system. The softening effects of saliva can be ignored during the first chewing cycle. However, as the chewing process goes on, the saliva secretion increases and its role becomes more dominant. As mentioned earlier in 3.4.3.1, the SPH method has been successfully applied to the multi-physics problems [59]. Therefore, it is safe to say that the SPH solid fracture formulation, used in the food breakdown model can be coupled to the SPH formulation for fluids, which represents the softening effects of saliva. This integrated model will be used to comprehensively study the human oral food processing system.

5.3.2 Integrating the food breakdown model into the biomechanical model of jaw

Previous research studies have employed a biomechanical model of jaw and jaw muscles in order to investigate the chewing dynamics [60] and neuromuscular control of jaw muscles [61]. Although the previous experimental studies have highlighted the effect of food hardness on the jaw muscle activity [62], the currently available biomechanical models of jaw have simplified the effect of the occlusal force to a constant force vector. This indicates that these biomechanical models cannot provide a thorough investigation of the masticatory system. By integrating the food breakdown model into the biomechanical model of jaw, the model will be ultimately able to represent a comprehensive simulation of chewing biomechanics and jaw dynamics. Upon setting a coupled relation between the occlusal force and the jaw dynamics, we will be able to use the measurements of jaw movements as an alternative way to investigate the validity of the occlusal force measurements.

From the experimental studies, it is commonly believed that mastication is a sensory motor activity. The sensory information from the food texture controls the muscle activity, and subsequently, the occlusal force. Although previous experiments have shown the difference in the amount of muscle activity while chewing hard and soft foods [62], the actual connection between the different control components is still unknown. A coupled food breakdown-jaw biomechanics model has the potential to study the neuromuscular control of human masticatory system.

The first step in integrating the food breakdown model into the biomechanical model of jaw, the SPH-FEM coupled formulation, has been covered as part of this research thesis (4.1).

5.3.3 Patient-specific mastication models

The current state of the art in the mandibular reconstructive surgery aims to reconstruct the natural geometry of the mandible using assistive technologies such as patient-specific computer-aided surgery. The clinician-rated post-operative investigations have shown health and life-quality improvements in patients following the mandibular reconstruction surgery [63]. However, the patient-based assessments indicate that around 63% of patients are not satisfied with the quality of their mastication following the reconstruction [64]. The contrast between the clinical outcomes and the patients' satisfaction highlights the need for a more function-based pre-assessment of the mandibular reconstruction. The food breakdown modeling approach represented in this thesis was able to assess the masticatory performance and the occlusal force correlatively; it ties the clinical outcome to what patients perceive. By integrating the medical imaging data into the biomechanical model of mastication, we will be able to build a patient-specific mastication model that can be considered as a promising tool to comprehensively evaluate the success of the surgical plan.

Bibliography

[1] G. Agerberg and G. E. Carlsson, “Chewing ability in relation to dental and general health: Analyses of data obtained from a questionnaire,” *Acta Odontol. Scand.*, 1981, doi: 10.3109/00016358109162273.

[2] A. van der Bilt, “Assessment of mastication with implications for oral rehabilitation: A review,” *J. Oral Rehabil.*, vol. 38, no. 10, pp. 754–780, 2011, doi: 10.1111/j.1365-2842.2010.02197.x.

[3] N. M. Oliveira, L. M. Shaddox, C. Toda, A. G. Paleari, A. C. Pero, and M. A. Compagnoni, “Methods for evaluation of masticatory efficiency in conventional complete denture wearers: a systematized review.,” *Oral Health Dent. Manag.*, vol. 13, no. 3, pp. 757–62, 2014.

[4] S. Okiyama, K. Ikebe, and T. Nokubi, “Association between masticatory performance and maximal occlusal force in young men,” *J. Oral Rehabil.*, 2003, doi: 10.1046/j.1365-2842.2003.01009.x.

[5] B. Dejak, A. Młotkowski, and M. Romanowicz, “Finite element analysis of stresses in molars during clenching and mastication,” *J. Prosthet. Dent.*, vol. 90, no. 6, pp. 591–597, 2003, doi: 10.1016/j.prosdent.2003.08.009.

[6] S. M. Harrison, G. Eyres, P. W. Cleary, M. D. Sinnott, C. Delahunty, and L. Lundin, “Computational modeling of food oral breakdown using smoothed particle hydrodynamics,” *J. Texture Stud.*, vol. 45, no. 2, pp. 97–109, 2014, doi: 10.1111/jtxs.12062.

[7] V. P. Nguyen, T. Rabczuk, S. Bordas, and M. Duflot, “Meshless methods: A review and

computer implementation aspects," *Mathematics and Computers in Simulation*. 2008, doi: 10.1016/j.matcom.2008.01.003.

[8] D. E. Grady and M. E. Kipp, "DYNAMIC ROCK FRAGMENTATION," in *Fracture Mechanics of Rock*, 1987.

[9] T. Witt and J. R. Stokes, "Physics of food structure breakdown and bolus formation during oral processing of hard and soft solids," *Curr. Opin. Food Sci.*, vol. 3, pp. 110–117, 2015, doi: 10.1016/j.cofs.2015.06.011.

[10] K. Matsuo and J. B. Palmer, "Anatomy and Physiology of Feeding and Swallowing: Normal and Abnormal," *Phys. Med. Rehabil. Clin. N. Am.*, vol. 19, no. 4, pp. 691–707, 2008, doi: 10.1016/j.pmr.2008.06.001.

[11] B. P. Pick, "Gray's Anatomy," *British Medical Journal*. 1958, doi: 10.1136/bmj.2.5099.801-e.

[12] Y. Matsui, K. Ohno, K. Michi, H. Hata, K. Yamagata, and S. Ohtsuka, "The evaluation of masticatory function with low adhesive colour-developing chewing gum," *Journal of Oral Rehabilitation*. 1996, doi: 10.1111/j.1365-2842.1996.tb00849.x.

[13] M. R. Heath, "The effect of maximum biting force and bone loss upon masticatory function and dietary selection of the elderly.," *Int. Dent. J.*, 1982.

[14] A. van der Bilt, H. W. van der Glas, F. Mowlana, and M. R. Heath, "A comparison between sieving and optical scanning for the determination of particle size distributions obtained by mastication in man," *Arch. Oral Biol.*, 1993, doi: 10.1016/0003-9969(93)90201-V.

[15] M. Bakke, B. Holm, and K. Gotfredsen, "Masticatory function and patient satisfaction with implant-supported mandibular overdentures: a prospective 5-year study.," *Int. J.*

Prosthodont., vol. 15, no. 6, pp. 575–81, 2002.

[16] K. Shala *et al.*, "Evaluation of maximum bite force in patients with complete dentures," *Open Access Maced. J. Med. Sci.*, 2018, doi: 10.3889/oamjms.2018.141.

[17] M. A. Peyron, C. Lassauzay, and A. Woda, "Effects of increased hardness on jaw movement and muscle activity during chewing of visco-elastic model foods," *Exp. Brain Res.*, 2002, doi: 10.1007/s00221-001-0916-5.

[18] C. H. Gibbs, P. E. Mahan, H. C. Lundeen, K. Brehnan, E. K. Walsh, and W. B. Holbrook, "Occlusal forces during chewing and swallowing as measured by sound transmission," *J. Prosthet. Dent.*, 1981, doi: 10.1016/0022-3913(81)90455-8.

[19] J. Chen, N. Khandelwal, Z. Liu, and T. Funami, "Influences of food hardness on the particle size distribution of food boluses," *Arch. Oral Biol.*, 2013, doi: 10.1016/j.archoralbio.2012.10.014.

[20] T. Sugiura, K. Fueki, and Y. Igarashi, "Comparisons between a mixing ability test and masticatory performance tests using a brittle or an elastic test food," *J. Oral Rehabil.*, 2009, doi: 10.1111/j.1365-2842.2008.01917.x.

[21] T. W. P. Korioth, D. P. Romilly, and A. G. Hannam, "Three-dimensional finite element stress analysis of the dentate human mandible," *Am. J. Phys. Anthropol.*, 1992, doi: 10.1002/ajpa.1330880107.

[22] J. H. Koolstra and T. M. G. J. Van Eijden, "Combined finite-element and rigid-body analysis of human jaw joint dynamics," *J. Biomech.*, 2005, doi: 10.1016/j.jbiomech.2004.10.014.

[23] P. W. LUCAS, D. A. LUKE, F. C. T. VOON, C. L. CHEW, and R. OW, "Food breakdown patterns produced by human subjects possessing artificial and natural teeth," *J.*

Oral Rehabil., 1986, doi: 10.1111/j.1365-2842.1986.tb00652.x.

[24] Y. Sun and W. L. Xu, “Simulation of food mastication based on Discrete Element Method,” *Int. J. Comput. Appl. Technol.*, 2010, doi: 10.1504/IJCAT.2010.034723.

[25] D. Francois, “Brittle fracture,” *Encycl. Dict. Polym.*, pp. 129–129, 2007, doi: 10.1007/978-0-387-30160-0_1559.

[26] D. Roylance, “Introduction to Fracture Mechanics,” pp. 1–17, 2001.

[27] A. A. Griffith, “The phenomena of rupture and flow in solids, Griffith.pdf,” *Philos. Trans. R. Soc. London*, 1921.

[28] J. Dolbow, N. Moës, and T. Belytschko, “Discontinuous enrichment in finite elements with a partition of unity method,” *Finite Elem. Anal. Des.*, 2000, doi: 10.1016/S0168-874X(00)00035-4.

[29] I. Babuška and J. M. Melenk, “The partition of unity method,” *Int. J. Numer. Methods Eng.*, 1997, doi: 10.1002/(SICI)1097-0207(19970228)40:4<727::AID-NME86>3.0.CO;2-N.

[30] R. A. Gingold and J. J. Monaghan, “Smoothed particle hydrodynamics: theory and application to non-spherical stars,” *Mon. Not. R. Astron. Soc.*, 1977, doi: 10.1093/mnras/181.3.375.

[31] P. W. Randles and L. D. Libersky, “Smoothed particle hydrodynamics: Some recent improvements and applications,” *Comput. Methods Appl. Mech. Eng.*, 1996, doi: 10.1016/S0045-7825(96)01090-0.

[32] J. Bonet and T. S. L. Lok, “Variational and momentum preservation aspects of Smooth Particle Hydrodynamic formulations,” *Comput. Methods Appl. Mech. Eng.*, 1999, doi: 10.1016/S0045-7825(99)00051-1.

[33] J. J. Monaghan, “Smoothed particle hydrodynamics,” *Reports on Progress in Physics*. 2005, doi: 10.1088/0034-4885/68/8/R01.

[34] J. W. Swegle, D. L. Hicks, and S. W. Attaway, “Smoothed particle hydrodynamics stability analysis,” *J. Comput. Phys.*, 1995, doi: 10.1006/jcph.1995.1010.

[35] G. R. Johnson, R. A. Stryk, and S. R. Beissel, “SPH for high velocity impact computations,” *Comput. Methods Appl. Mech. Eng.*, 1996, doi: 10.1016/S0045-7825(96)01089-4.

[36] C. T. Dyka, P. W. Randles, and R. P. Ingel, “Stress points for tension instability in SPH,” *Int. J. Numer. Methods Eng.*, 1997, doi: 10.1002/(SICI)1097-0207(19970715)40:13<2325::AID-NME161>3.0.CO;2-8.

[37] P. W. Randles and L. D. Libersky, “Normalized SPH with stress points,” *Int. J. Numer. Methods Eng.*, 2000, doi: 10.1002/1097-0207(20000810)48:10<1445::AID-NME831>3.0.CO;2-9.

[38] J. K. Chen, J. E. Beraun, and C. J. Jih, “An improvement for tensile instability in smoothed particle hydrodynamics,” *Comput. Mech.*, 1999.

[39] R. Das and P. W. Cleary, “Evaluation of Accuracy and Stability of the Classical SPH Method Under Uniaxial Compression,” *J. Sci. Comput.*, vol. 64, no. 3, pp. 858–897, 2015, doi: 10.1007/s10915-014-9948-4.

[40] Z. Mao, G. R. Liu, and X. Dong, “A comprehensive study on the parameters setting in smoothed particle hydrodynamics (SPH) method applied to hydrodynamics problems,” *Comput. Geotech.*, 2017, doi: 10.1016/j.compgeo.2017.07.024.

[41] K. Damaziak and J. Malachowski, “Comparison of SPH and FEM in thermomechanical coupled problems,” *AIP Conf. Proc.*, vol. 2078, no. March, 2019, doi: 10.1063/1.5092066.

[42] T. Jankowiak and T. Lodygowski, “Smoothed particle hydrodynamics versus finite element method for blast impact,” *Bull. Polish Acad. Sci. Tech. Sci.*, 2013, doi: 10.2478/bpasts-2013-0009.

[43] S. Mohammadi, *Extended Finite Element Method: For Fracture Analysis of Structures*. 2008.

[44] S. Sticko, “Smooth Particle Hydrodynamics Applied to Fracture Mechanics Mechanics,” *Master’s Thesis*, 2013.

[45] A. K. Ho, L. Tsou, S. Green, and S. Fels, “A 3D swallowing simulation using smoothed particle hydrodynamics,” *Comput. Methods Biomech. Biomed. Eng. Imaging Vis.*, 2014, doi: 10.1080/21681163.2013.862862.

[46] H. J. Melosh, E. V. Ryan, and E. Asphaug, “Dynamic fragmentation in impacts: hydrocode simulation of laboratory impacts,” *J. Geophys. Res.*, 1992, doi: 10.1029/92je01632.

[47] W. R. Wawersik and C. Fairhurst, “A study of brittle rock fracture in laboratory compression experiments,” *Int. J. Rock Mech. Min. Sci.*, 1970, doi: 10.1016/0148-9062(70)90007-0.

[48] G. Ma, H. Li, L. Yan, and L. Huang, “Testing and analysis of basalt FRP-confined damaged concrete cylinders under axial compression loading,” *Constr. Build. Mater.*, 2018, doi: 10.1016/j.conbuildmat.2018.02.172.

[49] M. Destrade, M. D. Gilchrist, J. Motherway, and J. G. Murphy, “Slight compressibility and sensitivity to changes in Poisson’s ratio,” *Int. J. Numer. Methods Eng.*, 2012, doi: 10.1002/nme.3326.

[50] G. Lube, H. E. Huppert, R. S. J. Sparks, and A. Freundt, “Collapses of two-dimensional

granular columns,” *Phys. Rev. E - Stat. Nonlinear, Soft Matter Phys.*, 2005, doi: 10.1103/PhysRevE.72.041301.

[51] Z. Zhang, H. Qiang, and W. Gao, “Coupling of smoothed particle hydrodynamics and finite element method for impact dynamics simulation,” *Eng. Struct.*, 2011, doi: 10.1016/j.engstruct.2010.10.020.

[52] K. R. Agrawal, “Mechancial properties of foods responsible for resisting food breakdown in the human mouth,” vol. 42, no. 1, pp. 1–9, 1997.

[53] A. P. SLAGTER, F. BOSMAN, and A. VAN DER BILT, “Comminution of two artificial test foods by dentate and edentulous subjects,” *J. Oral Rehabil.*, 1993, doi: 10.1111/j.1365-2842.1993.tb01599.x.

[54] C. Aydin, “Physical properties of almond nut and kernel,” *J. Food Eng.*, 2003, doi: 10.1016/S0260-8774(03)00053-0.

[55] A. Jahanbakhshi, Y. Abbaspour-Gilandeh, and T. M. Gundoshmian, “Determination of physical and mechanical properties of carrot in order to reduce waste during harvesting and post-harvesting,” *Food Sci. Nutr.*, 2018, doi: 10.1002/fsn3.760.

[56] C. Aydin, “Some engineering properties of peanut and kernel,” *J. Food Eng.*, 2007, doi: 10.1016/j.jfoodeng.2006.02.045.

[57] D. LUNDGREN and L. LAURELL, “Occlusal force pattern during chewing and biting in dentitions restored with fixed bridges of cross-arch extension: I. Bilateral end abutments,” *J. Oral Rehabil.*, 1986, doi: 10.1111/j.1365-2842.1986.tb01556.x.

[58] E. B. De Las Casas, A. F. De Almeida, C. A. Cimini, P. D. T. V. Gomes, T. P. M. Cornacchia, and J. M. E. Saffar, “Determination of tangential and normal components of oral forces,” *J. Appl. Oral Sci.*, 2007, doi: 10.1590/s1678-77572007000100015.

[59] C. Ulrich, M. Leonardi, and T. Rung, “Multi-physics SPH simulation of complex marine-engineering hydrodynamic problems,” *Ocean Eng.*, vol. 64, pp. 109–121, 2013, doi: 10.1016/j.oceaneng.2013.02.007.

[60] A. G. Hannam, I. Stavness, J. E. Lloyd, and S. Fels, “A dynamic model of jaw and hyoid biomechanics during chewing,” *J. Biomech.*, 2008, doi: 10.1016/j.jbiomech.2007.12.001.

[61] R. Laboissière, D. J. Ostry, and A. G. Feldman, “The control of multi-muscle systems: Human jaw and hyoid movements,” *Biol. Cybern.*, 1996, doi: 10.1007/BF00194930.

[62] K. R. Agrawal, P. W. Lucas, I. C. Bruce, and J. F. Prinz, “Food properties that influence neuromuscular activity during human mastication,” *J. Dent. Res.*, 1998, doi: 10.1177/00220345980770111101.

[63] K. M. Wilson, N. M. Rizk, S. L. Armstrong, and J. L. Gluckman, “Effects of hemimandibulectomy on quality of life,” *Laryngoscope*, 1998, doi: 10.1097/00005537-199810000-00028.

[64] F. Hölzle *et al.*, “Clinical outcome and patient satisfaction after mandibular reconstruction with free fibula flaps,” *Int. J. Oral Maxillofac. Surg.*, 2007, doi: 10.1016/j.ijom.2007.04.013.